© 2019. Published by The Company of Biologists Ltd | Development (2019) 146, dev179275. doi:10.1242/dev.179275

RESEARCH ARTICLE

Combover interacts with the axonemal component Rsp3 and is required for *Drosophila* sperm individualization

Josefa Steinhauer[1,*], Benjamin Statman[1], Jeremy K. Fagan[2], Jacob Borck[1], Satya Surabhi[2], Prathibha Yarikipati[2], Daniel Edelman[1] and Andreas Jenny[2,*]

ABSTRACT

Gamete formation is key to survival of higher organisms. In male animals, spermatogenesis gives rise to interconnected spermatids that differentiate and individualize into mature sperm, each tightly enclosed by a plasma membrane. In *Drosophila melanogaster*, individualization of sister spermatids requires the formation of specialized actin cones that synchronously move along the sperm tails, removing inter-spermatid bridges and most of the cytoplasm. Here, we show that Combover (Cmb), originally identified as an effector of planar cell polarity (PCP) under control of Rho kinase, is essential for sperm individualization. *cmb* mutants are male sterile, with actin cones that fail to move in a synchronized manner along the flagella, despite being correctly formed and polarized initially. These defects are germline autonomous, independent of PCP genes, and can be rescued by wild-type Cmb, but not by a version of Cmb in which known Rho kinase phosphorylation sites are mutated. Furthermore, Cmb binds to the axonemal component Radial spoke protein 3, knockdown of which causes similar individualization defects, suggesting that Cmb coordinates the individualization machinery with the microtubular axonemes.

KEY WORDS: Spermatogenesis, Individualization, Axoneme, Planar cell polarity, Combover, Rho kinase

INTRODUCTION

Proper differentiation of germline cells into eggs and sperm is essential for the perpetuation of a species. Sperm cells in mammals and *Drosophila melanogaster* develop from germline stem cells that produce mitotic spermatogonia, which ultimately undergo meiosis and terminal spermatid differentiation. *Drosophila* has long been a powerful model organism for studying spermiogenesis, which begins after meiosis, when the syncytial spermatids derived from a single gonialblast (the differentiating stem cell daughter; Fig. 1A) begin morphological changes required for their differentiation, including mitochondrial differentiation, flagellar elongation, nuclear compaction and acrosome formation (reviewed by Fabian and Brill, 2012; Fuller, 1993; Hermo et al., 2010a,b). In *Drosophila*, after meiosis is completed, mitochondria aggregate around the basal body on one side of the nucleus. Subsequently, the mitochondria fuse to form the 'Nebenkern' (Tokuyasu, 1975). As differentiation proceeds, spermatids form acrosomes, their nuclei remodel and compact, and sperm tails (flagella) elongate (Fig. 1A,B). During spermatid elongation, both axonemal microtubules (MTs) and the mitochondrial Nebenkern extend to form the flagellum, composed of a central axoneme flanked by major and minor mitochondrial derivatives (Fuller, 1993). *Drosophila* sperm axonemes are structurally similar to other axonemes, containing a central MT pair ringed by nine outer MT doublets (Fabian and Brill, 2012).

In *Drosophila*, as in mammals, incomplete cytokinesis during sperm development leads to cytoplasmic sharing between sister spermatids (Greenbaum et al., 2011). Following terminal differentiation, the inter-spermatid cytoplasmic bridges are dissolved and the spermatids' cytoplasmic contents are removed (Fabrizio et al., 1998; Tokuyasu et al., 1972a). This process in *Drosophila*, called individualization, is carried out by the actin-rich individualization complex (IC) that first forms adjacent to the needle-shaped spermatid nuclei, which by this point are clustered in the basal testis (Fig. 1B,C). The IC is composed of 64 actin cones, one for each spermatid nucleus of the germline cyst (Fabrizio et al., 1998; Tokuyasu et al., 1972a), and it shares similarities with actin comets found on endocytic vesicles (Bazinet and Rollins, 2003). As individualization proceeds, the actin cones of the IC move synchronously away from the nuclei toward the apical domain of the testis (Fig. 1B), traversing the spermatid tails (Fig. 1C, arrowheads) until they reach the end of the flagella (Noguchi and Miller, 2003). Each moving IC generates a growing cystic bulge that contains the extruded cytoplasmic contents of the individualizing cyst. When the IC and associated cystic bulge reach the end of the flagella, they form a waste bag (WB) full of discarded organelles (Fig. 1C, arrow), degradation of which may occur by an apoptosis-like program (Arama et al., 2003; Huh et al., 2004; Tokuyasu et al., 1972a). As a result of individualization, each streamlined spermatozoon resides within its own plasma membrane, most of its cytoplasm has been extruded, and it no longer maintains connections to its sister spermatids (Tokuyasu et al., 1972a). Once this process has been completed, mature sperm are coiled in preparation for release into the seminal vesicle, and WBs and abnormal sperm are eliminated within the base of the testis (Tokuyasu et al., 1972b).

Elegant prior studies have provided a detailed view of the polarized IC structure. At the leading edge of the actin cones, F-actin filaments form a meshwork under the control of the Arp2/3 actin-nucleating complex (Noguchi et al., 2008; Rogat and Miller, 2002), whereas at their rear, F-actin is organized into parallel bundles by the activity of the actin-bundling proteins Quail/Villin, Chickadee/Profilin and Singed/Fascin (Noguchi et al., 2006, 2008). IC activities are thought to be segregated, with the front meshwork being responsible for cytoplasmic extrusion and the rear bundles responsible for movement along the sperm tails. During individualization, cones accumulate actin (Noguchi et al., 2006,

[1]Department of Biology, Yeshiva University, New York, NY 10033, USA. [2]Department of Developmental and Molecular Biology and Department of Genetics, Albert Einstein College of Medicine, New York, NY 10461, USA.

*Authors for correspondence (jsteinha@yu.edu; andreas.jenny@einstein.yu.edu)

J.S., 0000-0002-0960-5271; B.S., 0000-0001-8134-6895; J.K.F., 0000-0003-0681-9845; J.B., 0000-0002-2692-8523; D.E., 0000-0002-0236-6829; A.J., 0000-0001-5989-8212

Received 10 April 2019; Accepted 24 July 2019

Development (2019) 146, dev179275. doi:10.1242/dev.179275

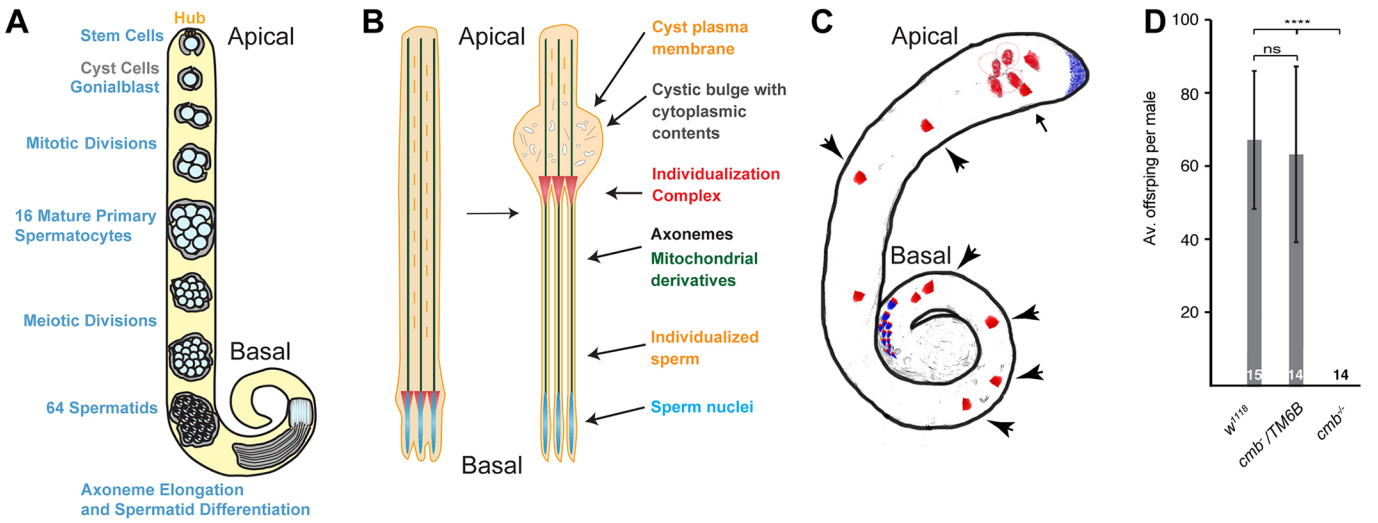

Fig. 1. *cmb* mutants are male sterile. (A) Schematic of spermatogenesis in *Drosophila.* Germline and somatic stem cells reside at the apical tip of the testis tube in a niche called the hub. Asymmetric division of stem cells produces a differentiating germline gonialblast that is surrounded by two somatic cyst cells, which do not divide further. Differentiating germline spermatogonia, derived from the gonialblast, undergo four mitotic divisions to yield 16 primary spermatocytes, followed by two meiotic divisions. Cytokinesis of each division is incomplete, allowing the 64 sister spermatids to share cytoplasm via ring canals. Newly forming cysts push older cysts basally in the testis tube. Following meiosis, the mitochondria of each spermatid aggregate to form the Nebenkern, which subsequently elongates along with the axoneme to form the sperm tail. In spermiogenesis, sperm tails extend back toward the apical testis tip, pushing the spermatid nuclei basally within the testis tube, and spermatid nuclei become highly compacted, taking on their characteristic needle shape. (B) At the end of spermiogenesis, actin-rich individualization complexes form around bundled spermatid nuclei in the basal region of the testis and move along the sperm tails toward the apical region, extruding cytoplasmic contents into cystic bulges as they move. After individualization, each individualized sperm lacks most cytoplasm, no longer shares ring canals with its sisters, and is invested in its own plasma membrane. Adapted from Steinhauer (2015). (C) Drawing of a testis showing the position of basally forming ICs in contact with nuclei (blue), as well as mature, apically moving ICs (red; arrowheads) and normal WBs (arrow). Adapted from Ben-David et al. (2015). (D) Compared with wild-type (w^{1118}) and heterozygous ($cmb^{-}/TM6B$) siblings, homozygous mutant cmb^{KO} males produce no progeny when mated to wild-type females. Error bars represent s.d.; one-way ANOVA (P<0.0001) and Tukey's multiple comparisons test (****P<0.0001). ns, not significant.

2008), and actin polymerization, but not myosin motor activity, is essential for IC progression (Mermall et al., 2005; Noguchi et al., 2006, 2008; Noguchi and Miller, 2003; Tokuyasu et al., 1972a; reviewed by Steinhauer, 2015).

We previously identified *combover* (*cmb*), a gene encoding two major protein isoforms that are predicted to be largely intrinsically disordered (Mészáros et al., 2018) and lack any known domains, as a Rho kinase substrate that acts as a planar polarity effector (PPE) to affect *Drosophila* wing hair (trichome) formation (Fagan et al., 2014). During pupal development, each cell of the fly wing forms an actin-rich hair, surrounded by membrane, that points towards the distal tip of the wing (reviewed by Adler and Wallingford, 2017; Butler and Wallingford, 2017; Maung and Jenny, 2011). Polarized wing hair formation is governed by the non-canonical Wnt-planar cell polarity (PCP) pathway (reviewed by Adler and Wallingford, 2017; Butler and Wallingford, 2017; Maung and Jenny, 2011), during which core PCP proteins including Frizzled (Fz), Dishevelled (Dsh), Van Gogh (Vang), Prickle (Pk), Diego (Dgo), and Flamingo (Starry night) localize asymmetrically across proximal-distal wing cell borders. PCP-generated asymmetry leads to proximal enrichment of the PPE proteins Inturned, Fuzzy, Fritz and Multiple wing hairs (Mwh), which prevent ectopic wing hair formation (Adler et al., 2004; Strutt and Warrington, 2008). Additionally, Mwh prevents the formation of multiple prehairs, and it bundles actin to restrict hair formation to a single hair during trichome outgrowth (Lu et al., 2015). Although *cmb* mutants show no wing phenotype, Cmb overexpression causes formation of a multiple hair cell (MHC) phenotype that is enhanced by removal of one gene dose of *Rok* or the PPE genes, including *mwh* (Fagan et al., 2014). Indeed, the two major isoforms of Cmb, PA and PB, physically interact with Mwh, and the MHC phenotype observed in *mwh* single mutants is partially suppressed in *mwh cmb* double mutants. It was therefore suggested that Cmb promotes actin-based wing hair formation under control of Rok, a function that is antagonized by Mwh (Fagan et al., 2014).

We noticed that *cmb* mutants are male sterile. Here, we find that this is due to a requirement for *cmb* in the germline, in the actin-based process of spermatid individualization. Detailed histochemical and electron microscopic analyses of *cmb* mutant testes show that early cyst formation is normal. Furthermore, ICs form normally and start to move but do not remain properly aligned, and, although they initially recruit actin at normal levels, they fail to maintain and accumulate actin during IC progression. Despite evidence that Cmb affects actin-related processes (wing hair formation in the pupa and individualization of sperm), Cmb does not directly interact with actin in co-immunoprecipitation (CoIP) or co-sedimentation assays. Furthermore, we show that the role of *cmb* during individualization is independent of and distinct from PCP genes. Significantly, Cmb interacts with the axonemal component Radial spoke protein 3 (Rsp3/CG32392), knockdown of which causes individualization phenotypes highly similar to those of *cmb* mutants, suggesting that Cmb coordinates IC movement with the axoneme during biogenesis of functional sperm.

RESULTS

Spermatid individualization is abnormal in *cmb* mutants

cmb mutant males were completely sterile, as individual homozygous cmb^{KO} ($cmb^{-/-}$) males (Fagan et al., 2014) crossed to w^{1118} females reproducibly did not yield progeny, in contrast to wild-type or heterozygous males, which gave rise to an average of

Development (2019) 146, dev179275. doi:10.1242/dev.179275

67±19 and 63±24 offspring per male, respectively (Fig. 1D). To investigate the cause of the male sterility, testes from *cmb* mutants were examined cytologically for each stage of spermatogenesis. α-Spectrin staining revealed normal round spectrosomes in the germline stem cells and gonialblasts (compare arrowheads in sibling controls with homozygous cmb^{KO} mutants in Fig. 2A and 2B, respectively), as well as normal branched fusomes in mitotic spermatogonia (Fig. 2A,B, arrows) of *cmb* mutants, suggesting that initial germline divisions are normal. Consistent with this, ring canals connecting the spermatogonia and spermatocytes appeared normal (Fig. S1). Phase-contrast imaging of squashed testes was used to visualize spermatids following meiosis (Fig. 2C,D). Each phase-light nucleus (Fig. 2D, arrowhead) was accompanied by a phase-dark mitochondrial Nebenkern of similar size (Fig. 2D, arrow) in cmb^{KO} spermatids, indicating normal meiotic cytokinesis. Following meiosis, spermatid elongation was normal in homozygous cmb^{KO} mutants, as assessed by the presence of normal elongation complexes at the ends of the spermatid tails, decorated with α-Spectrin (Fig. 2E,F; Ghosh-Roy et al., 2004), and compacted bundled spermatid nuclei were visible in the basal region of cmb^{KO} mutant testes (e.g. Fig. 2I,J, DAPI). Several other aspects of spermiogenesis in *cmb* mutants also proceeded normally, including cytoplasmic caspase activation (Fig. 2G,H) and initial formation of ICs around the bundled spermatid nuclei (Fig. 2I,J, arrowheads; see also below and Fig. 5A-C). However, in *cmb* mutants the seminal vesicles were empty, indicating the absence of mature sperm (compare heterozygote in Fig. 2K with homozygous mutant in 2L).

Despite apparently normal IC formation and caspase activation in cmb^{KO} mutants, the advancement of spermatid individualization was highly perturbed. In wild-type or heterozygous *cmb* testes, the actin cones of each IC progressed synchronously towards the end of the sperm tails, ultimately forming WB structures in the apical domain of the testis (Fig. 3A; normal ICs and WBs quantified in Fig. 3I, as described in Ben-David et al., 2015; see Fig. 1B,C for schematics). In contrast, in cmb^{KO} mutants, ICs became scattered and disorganized as they progressed along the spermatid tails away from the bundled nuclei (Fig. 3B). Whereas wild type and

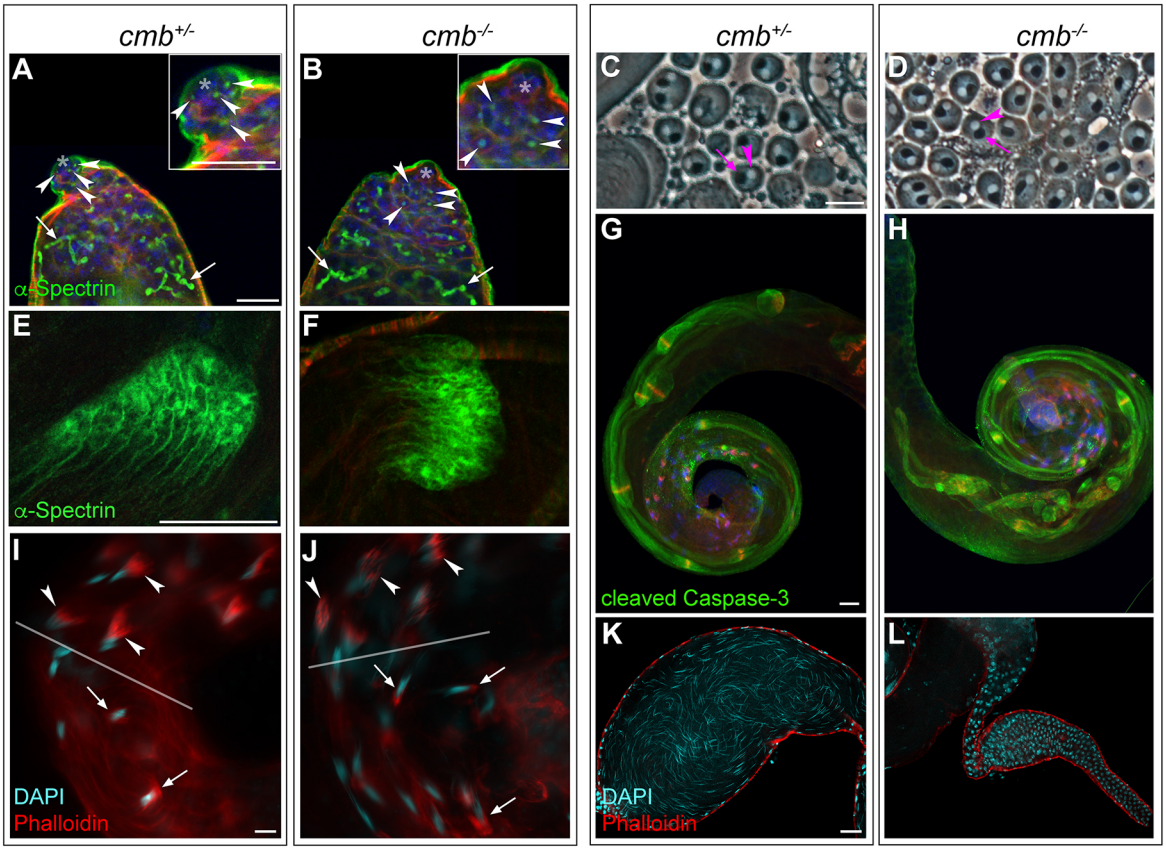

Fig. 2. Spermatogenesis in *cmb* mutants. (A,B) Staining against α-Spectrin (green) reveals the round spectrosomes of the germline stem cells and gonialblasts (arrowheads), as well as the branched fusomes of the mitotic spermatogonia (arrows). These early stages appear normal in the cmb^{KO} homozygotes (B, compare with heterozygous siblings in A). Insets in A and B show magnified spectrosomes in the germline stem cells and gonialblasts. Asterisks indicate apical hubs. Nuclei are in blue (DAPI), cell cortices in red (phalloidin). (C,D) Phase-contrast imaging of post-meiotic spermatids shows normal mitochondrial aggregation into Nebenkerne (arrows) in the cmb^{KO} homozygotes (D, compare with heterozygous siblings in C). Arrowheads indicate spermatid nuclei. Each Nebenkern is found in proximity to a similarly sized nucleus. (E,F) In addition to marking the spectrosomes and fusomes of the early germ cells, α-Spectrin staining (green) also decorates the elongation complexes at the tips of the elongating flagella. Elongation complexes appear normal in cmb^{KO} homozygotes (F) compared with heterozygotes (E). (G,H) Cytoplasmic caspases (green) are activated during individualization in both cmb^{KO} homozygotes (H) and heterozygotes (G). (I,J) cmb^{KO} mutants form ICs (phalloidin, red) normally (arrowheads in J, sibling controls shown in I) adjacent to spermatid nuclear bundles (DAPI, cyan). Sperm heads appear tightly packaged and properly surrounded by actin caps within the somatic head cyst cells in the basal testis where mature sperm coiling occurs (arrows in J; note that somatic actin caps are different from germline ICs). (K,L) cmb^{KO} mutants make no mature sperm (L, DAPI), and only the round somatic nuclei of the seminal vesicle walls are visible. Sibling control with mature needle-shaped sperm nuclei in the seminal vesicle is shown in K. DAPI (blue/cyan) highlights nuclei, and phalloidin stains actin (red) in fluorescence images. Scale bars: 20 µm (A-H,K,L); 10 µm (I,J).

Development (2019) 146, dev179275. doi:10.1242/dev.179275

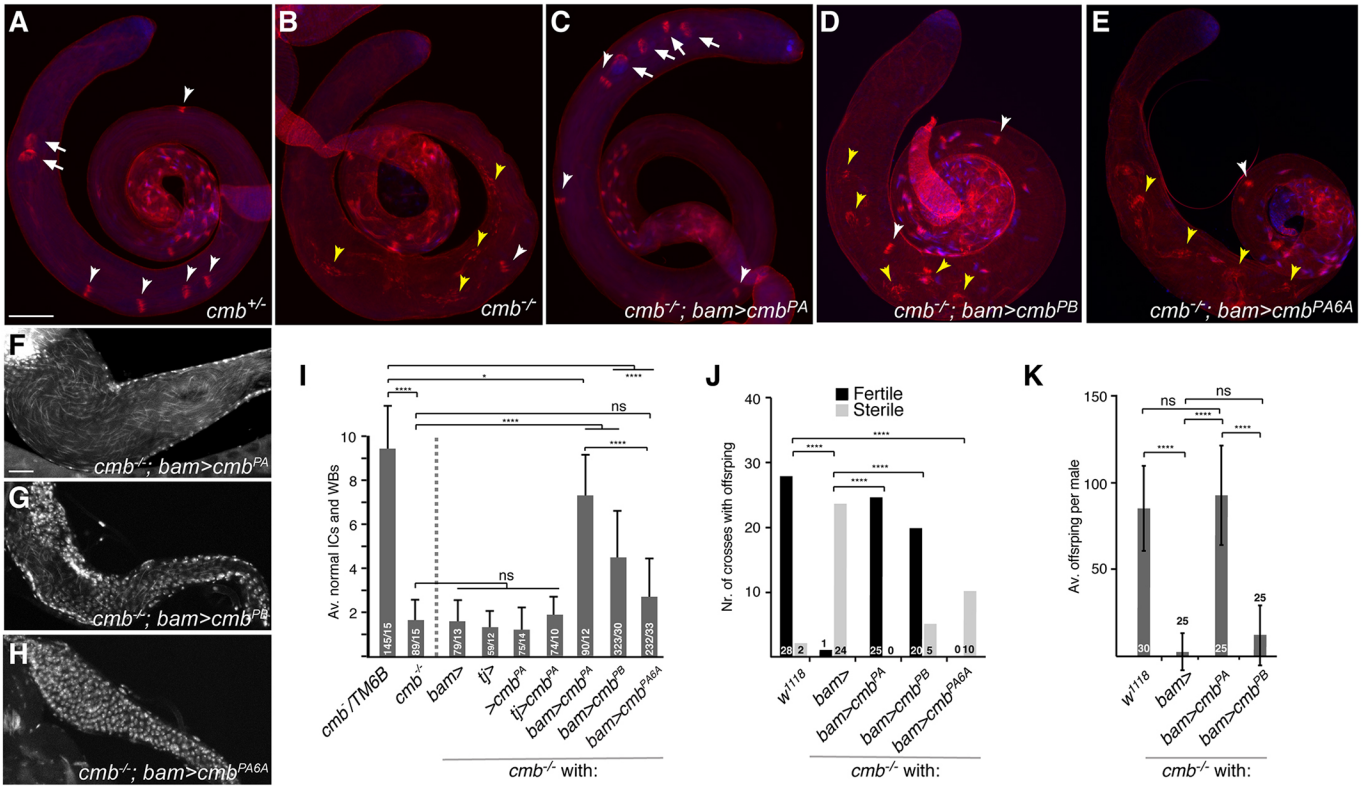

Fig. 3. *cmb* mutants show individualization defects, which can be rescued by germline expression of Cmb. (A,B) In control testes (A), intact ICs (white arrowheads) move along sperm tails from basal to apical and collect in WBs in the apical region (arrows). In cmb^{KO} mutant testes (B), nearly all ICs are scattered (yellow arrowheads) and WBs do not form. (C) ICs of cmb^{KO} mutants (white arrowheads) and WBs (arrows) are rescued by expression of Cmb-PA with the germline-specific driver *bam-GAL4*. (D) Germline expression (*bam-GAL4*) of Cmb-PB rescues some (white arrowheads) but not all (yellow arrowheads) ICs. (E) Germline expression (*bam-GAL4*) of the phosphoserine/threonine mutant transgene Cmb-PA6A does not rescue the ICs (yellow arrowheads) of cmb^{KO} mutants. In A-E, phalloidin staining (red) marks the ICs and DAPI (blue) marks the nuclei. Scale bar: 100 µm. (F-H) DAPI highlights the mature sperm nuclei in the seminal vesicles with Cmb-PA rescue (F) and Cmb-PB rescue (G). Note the presence of fewer mature sperm with Cmb-PB rescue compared with Cmb-PA. With the Cmb-PA6A rescue (H), no needle-shaped sperm nuclei are present, and only round somatic nuclei are visible. Scale bar: 20 µm. (I) Quantification of normal ICs and WBs. Germline expression of Cmb-PA largely rescues the individualization defect, whereas Cmb-PB rescues only partially. Germline expression of Cmb-PA6A does not rescue. For each genotype, at least 50 individualization structures were counted in a minimum of ten testes, as indicated by the numbers on the bars (number of total ICs and WBs/number of testes). Dotted vertical line separates the rescue experiments. (J,K) Germline expression of Cmb-PA also rescues the sterility of cmb^{KO} mutant males, as indicated by the number of fertile crosses from individual males (J) and the average number of progeny produced from single crosses (K). Germline expression of Cmb-PB rescues fertility only partially, and Cmb-PA6A does not rescue. Numbers on the bars in J indicate number of individual crosses that gave progeny (black bars) or that gave no progeny (gray bars). Numbers in K indicate the number of individual crosses contributing to the averages shown. Note that, surprisingly, the single escaper male carrying only *bam-GAL4* in the cmb^{KO} mutant background (the only one we ever found) was fully fertile. Error bars in I,K represent s.d. I,K: one-way ANOVA (P<0.001) and Tukey's multiple comparisons test. J: Fisher's Exact test. ****P<0.0001; *P<0.05. ns, not significant.

heterozygous sibling controls showed 8-11 normally progressing ICs and WBs per testis on average (see also Ben-David et al., 2015), cmb^{KO} mutants averaged fewer than two normally progressing ICs per testis (Fig. 3I). Together, our data demonstrate that male germline cells proceed through spermatogenesis normally until the individualization stage in *cmb* mutants. Individualization is initiated, with ICs forming and caspases being activated, but IC movement is abnormal. The individualization defect most likely explains the male sterility of the mutant.

Cmb is required in the germline for sperm individualization

The *cmb* gene encodes four transcripts. The three longer transcripts differ only slightly, with *cmb-RA* retaining an intron that is removed in *cmb-RC* and *cmb-RD*, and all three encode very similar protein isoforms (Fagan et al., 2014). The shortest transcript, *cmb-RB*, encodes a short Cmb-PB protein isoform that is fully contained within the long isoform Cmb-PA, and both of these isoforms cause similar MHC phenotypes when overexpressed in the wing (see also Fig. S3C for schematic; Fagan et al., 2014). In order to test whether Cmb is required in the germline or the soma and to confirm that the sterility phenotype is indeed due to loss of *cmb*, we performed rescue experiments specifically re-expressing the Cmb-PA and Cmb-PB isoforms in soma or germline exclusively using *traffic jam-GAL4* (*tj>*) and *bag of marbles-GAL4* (*bam>*), respectively (Siddall and Hime, 2017; White-Cooper, 2012). Expression of the PA isoform in the male germline resulted in robust rescue of both the fertility and individualization phenotypes of *cmb* mutants (Fig. 3C,F,I-K), whereas expression in the somatic cyst cells did not rescue (individualization phenotype quantified in Fig. 3I). In contrast, expression of the PB isoform only partially rescued fertility: although 20 of 25 single male crosses produced offspring, their number was much lower than in the case of rescue with Cmb-PA (Fig. 3J,K). Consistent with this, quantification of ICs showed that individualization was only partially rescued (Fig. 3D,I) and few mature sperm were observable in the seminal vesicles (Fig. 3G). Expression of each transgene was confirmed by immunofluorescence

Development (2019) 146, dev179275. doi:10.1242/dev.179275

(Fig. S2A-C). Note that overexpression of Cmb-PA or Cmb-PB in wild-type males did not cause any defects and thus the remaining fertility defects in *bam>cmb-PB* testes were not due to a gain-of-function or dominant-negative effect (not shown).

Cmb is a phosphorylation target of Rho kinase *in vitro* (Fagan et al., 2014). We were unable to assess directly a phenotype of *Rho kinase* (*Rok*) mutants in the male germline as *Rok* is on the X chromosome, making it impossible to generate germline clones, and neither RNAi-mediated knockdown nor the expression of a kinase-dead form of Rok resulted in a spermatogenesis defect. In addition, overexpressing a dominant-negative RhoA (Rho1), the GTPase that activates Rok (Winter et al., 2001), resulted in scattered spermatid nuclei and highly abnormal ICs, likely as a consequence of pleiotropic, earlier defects (Fig. S2F). Nevertheless, mutation of the five phospho-acceptor serines/threonines to alanines (including an additional sixth, neighboring threonine; Fagan et al., 2014) abrogated the rescuing activity of Cmb-PA (Fig. 3E,H-J; Fig. S2C). Altogether, we conclude that the longer PA isoform is essential for spermatid individualization and suggest that its phosphorylation is important in this process.

Electron microscopy confirmed the individualization phenotype of cmb^{KO} mutants. In pre-individualization spermatids, mitochondrial derivatives and axonemes were normal (Fig. 4A,B). However, in contrast to the fully individualized spermatids devoid of cytoplasm seen in wild-type control testes (Fig. 4C,E), *cmb* mutant spermatids at the individualization stage, recognized by the dense crystalline array within the major mitochondrial derivatives, were still surrounded by cytoplasm (Fig. 4D,F). Defects were also observed in reduction of the minor mitochondrial derivatives, which appeared enlarged relative to wild type at comparable stages (Fig. 4C,D, arrows), a characteristic of individualization failure (Tokuyasu et al., 1972a). Axonemes remained normal in *cmb* mutant spermatids at the individualization stage (Fig. 4F, compare with control in 4E). Despite the high penetrance of individualization defects in *cmb* mutants, some cysts displayed a mixture of both improperly and properly individualized spermatids (Fig. 4G, enlarged in 4H), a situation not found in wild type (Tokuyasu et al., 1972a). Altogether, our data suggest that spermatid individualization is the primary defect in *cmb* mutant testes.

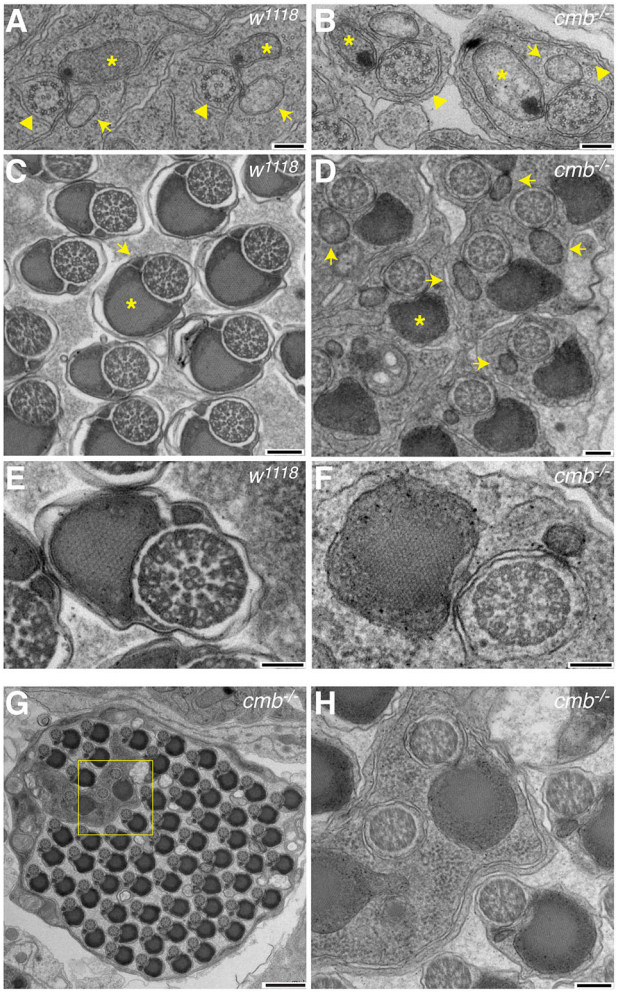

Fig. 4. *cmb* mutants show individualization defects. Electron micrographs of testis sections. A,C,E: w^{1118}; B,D,F-H: cmb^{KO}. (A,B) Preindividualization, axonemes and major and minor mitochondrial derivatives form normally in cmb^{KO} mutant cysts (arrowheads, asterisks and arrows, respectively). (C-F) Cysts of w^{1118} testes properly individualize, as seen by single units of axonemes, crystalline major (asterisks) and small minor (arrows) mitochondrial derivatives surrounded by plasma membrane (C; single spermatid enlarged in E), compared with spermatids of cmb^{KO} mutant cysts, which often fail to individualize and show variably sized minor mitochondrial components in syncytia (D; enlarged example in F). (G,H) Example of a cmb^{KO} cyst that partially failed to individualize, with boxed area in G enlarged in H. Scale bars: 200 nm (A-F,H); 2 µm (G).

Actin cones are structurally defective in *cmb* mutants

In addition to being scattered, *cmb* mutant ICs showed structural defects. Actin cones still associated with spermatid nuclei were not obviously aberrant and contained normal levels of actin (Fig. 5A,B; actin intensity quantified in Fig. 5C; see also schematics in Fig. 1B,C), suggesting that ICs initially formed normally. However, once they had moved away from the nuclei, most ICs in the *cmb* mutant were abnormal, and WBs containing the expunged cytoplasm were rarely found (quantified in Fig. 5D). Abnormalities among the *cmb* mutant ICs included reduced phalloidin staining, suggesting lower actin levels, and scattered actin cones (compare heterozygote in Fig. 5E with mutant in 5F and 5G). In some instances, *cmb* mutant actin cones appeared to lack their front flat edges, showing an abnormal needle-shaped morphology (Fig. 5H). In other cases, *cmb* mutant cones were shorter than normal and appeared to lack their rear tails (Fig. 5I). Elongated, needle-shaped actin cones are reminiscent of those observed in *Arp3* (a member of the Arp2/3 complex required for the formation of branched actin structures) mutants, whereas shorter ICs are similar to those observed in mutants of the actin-bundling genes *fascin* (*singed*) and *villin* (*quail*) (Noguchi et al., 2008).

To characterize further the actin cones in the *cmb* mutant, we examined other cone-associated proteins. Myosin VI (Jar) localizes to the front edges of the cones, where it is thought to be involved in organizing the meshwork of actin filaments (Fig. 6A-A″; Noguchi et al., 2006, 2008). *cmb* mutant cones still contained Myosin VI, even when phalloidin staining was strongly reduced (Fig. 6B-B″). Similarly, the actin-bundling proteins Quail and Singed, which localize to the rear tails of the actin cones (Fig. 6C-C″,E-E″; Noguchi et al., 2008), were still present in roughly the right position in *cmb* mutant cones, even when cone morphology was abnormal (Fig. 6D-D″,F-F″). Cones associated with spermatid nuclei were organized normally, with a rear domain marked by Singed protein and a front domain free of Singed staining (compare heterozygote in Fig. 6G-G″ with mutant in 6H-H″). Thus, the main defect in *cmb* mutants is abnormal actin accumulation and/or maintenance in individualization cones as the ICs progress along the spermatid tails.

As actin is aberrant in ICs of *cmb* mutants, we tested whether Cmb could bind actin in CoIP and co-sedimentation assays. As seen in Fig. S3A, neither GFP-tagged Cmb-PA nor Cmb-PB was able to

Development (2019) 146, dev179275. doi:10.1242/dev.179275

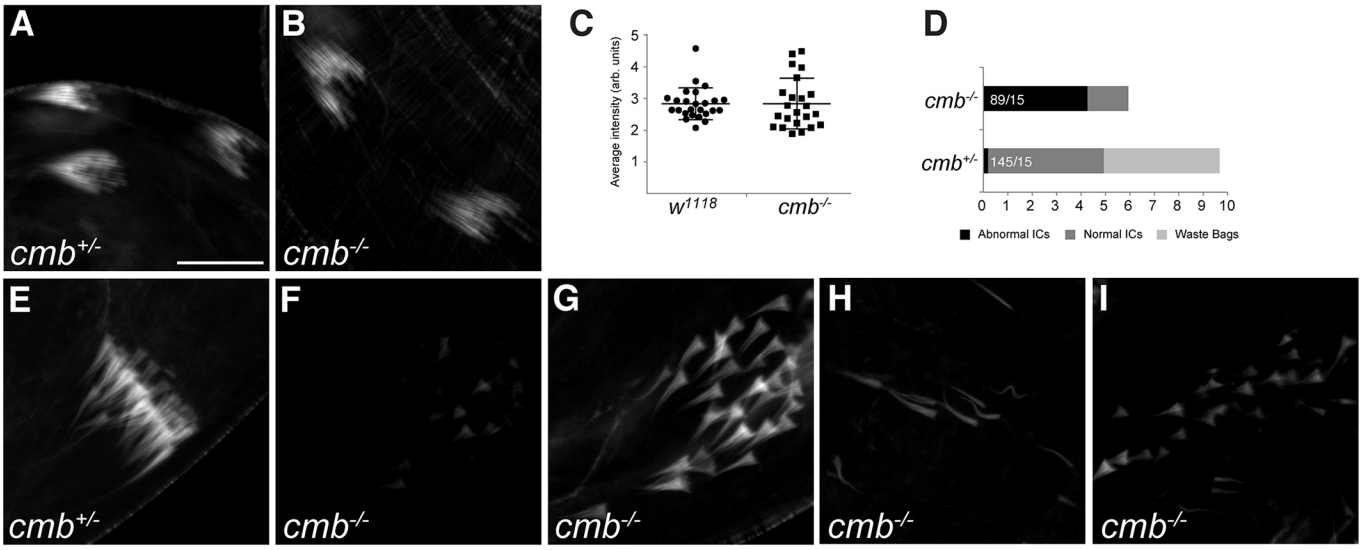

Fig. 5. *cmb* mutant ICs are abnormal. (A,B) cmb^{KO} mutant ICs (B) form normally around the spermatid nuclei in the basal region of the testis (compare with sibling controls in A). (C) Quantification of mean average intensity of phalloidin staining of early ICs still associated with nuclei shows that initial actin levels are normal in *cmb* mutants. (D) However, once ICs move away from the nuclei, they become predominantly abnormal in cmb^{KO} mutants [quantification shows average number of abnormal ICs (black), normal ICs (dark gray) and WBs (light gray) per testis; numbers indicate total number of individualization structures counted/number of testes counted]. (E-G) Abnormal ICs in cmb^{KO} mutants show less actin than wild type (F, compare with E, photographed on the same confocal settings) and are scattered (G, same IC as shown in F, photographed with higher laser gain). They can comprise actin cones lacking their front edges (H) or lacking their rear actin bundles (I). Phalloidin stains ICs in all micrographs. Scale bar: 20 µm.

co-immunoprecipitate V5-tagged actin from transfected HEK293 cells. We then tested purified, overlapping GST-tagged subfragments of Cmb-PB that had been used previously to map Rok phosphorylation sites (see schematic in Fig. S3C) (Fagan et al., 2014) for direct binding to muscle actin. The C-terminal GST-SX fragment was not soluble after a 150,000 ***g*** preclearing centrifugation, and neither GST-Cmb-ES nor GST-Cmb-BB co-sedimented with actin (compare supernatant and pellet fractions with the αActinin positive control in Fig. S3B). Thus, our experiments indicate that Cmb likely does not directly interact with actin.

Cmb may provide a link between axonemes and the IC

Two-hybrid analyses have shown that Cmb can interact with the Radial spoke protein Rsp3 (CG32392) and Pka-R1 (CG42341), the type 1 regulatory subunit of Protein kinase A, two proteins that also have been shown to interact with each other in the same study (Hu et al., 2017; Thurmond et al., 2019). Rsp3 dimers form an assembly scaffold for the radial spokes connecting the outer MT doublets to the central MT pair of axonemes (Huang et al., 1981; Luck et al., 1977; Porter and Sale, 2000; Wirschell et al., 2008; Yang et al., 2006). Rsp3 also is a Pka-anchoring protein (AKAP) in *Chlamydomonas* and vertebrates and is known to interact with Pka (Gaillard et al., 2001, 2006; Jivan et al., 2009). Indeed, we found that Rsp3 and Cmb-PA co-immunoprecipitated from HEK293 cells (Fig. S4).

Intriguingly, RNAi-mediated knockdown of *rsp3* with two independent, non-overlapping RNAi constructs caused IC phenotypes similar to those of *cmb* mutants (compare control in Fig. 7A with knockdowns in 7B,C). Specifically, ICs were scattered, and the number of normal ICs and WBs were reduced by more than 50% (quantification in Fig. 7E). Similarly, as with *cmb* mutants, the percentage of total ICs that had abnormal morphology was dramatically elevated compared with controls (Fig. 7F). As in *cmb* mutants (Fig. 2L), no mature sperm were found in seminal vesicles (compare control in Fig. 7G with 7H,I). Furthermore, one of the two available RNAi lines targeting Pka-R1 also reduced ICs and WBs, although with weaker expressivity (Fig. 7D,E; it did not increase the number of abnormal ICs to a statistically significant level; Fig. 7F). In that case though, mature sperm formed (Fig. 7J). Similar results were obtained upon co-expression of Dcr2 to enhance the knockdown efficiency (not shown). Importantly, acetylated (stable) α-tubulin staining was normal in elongated spermatids in all knockdown genotypes (Fig. 7K-N) and *cmb* mutants (Fig. 7O). In light of the known function of Rsp3, the similarity between the phenotypes suggest that Cmb, Rsp3 and Pka-R1 link the ICs to the axonemes in a manner that is required for proper IC progression and stability.

PCP genes are not required for spermatid individualization

Because *cmb* acts as an effector downstream of the PCP pathway in the wing (Fagan et al., 2014) and PCP genes are known to affect spermiogenesis in mammals (Chen and Cheng, 2016; Chen et al., 2016), we tested whether PCP genes were expressed in testes and were required for fertility or spermatid individualization. By qPCR, core PCP genes *frizzled* (*fz*), *diego* (*dgo*) and *prickle* (also known as *spiny leg*) were expressed at much lower levels in testes compared with imaginal discs, where they are known to be required (Fig. S5A) (Adler and Wallingford, 2017; Butler and Wallingford, 2017; Maung and Jenny, 2011). In contrast, *Van Gogh* (*Vang*), *Rok* and *mwh* were expressed at comparable levels, whereas *dishevelled* (*dsh*) and *cmb* were expressed at much higher levels in testes than in imaginal discs (Fig. S5A,B). None of the PCP genes tested showed reduced fertility in single male crosses, except, to our surprise, the PCP-specific, viable allele dsh^{1} (Fig. S6A), a phenotype that, to our knowledge, has not been reported previously (note though that the number of offspring of fertile dsh^{1} males was not different from wild type; Fig. S6B). The reduced fertility of dsh^{1} males was partially rescued by expression

Development (2019) 146, dev179275. doi:10.1242/dev.179275

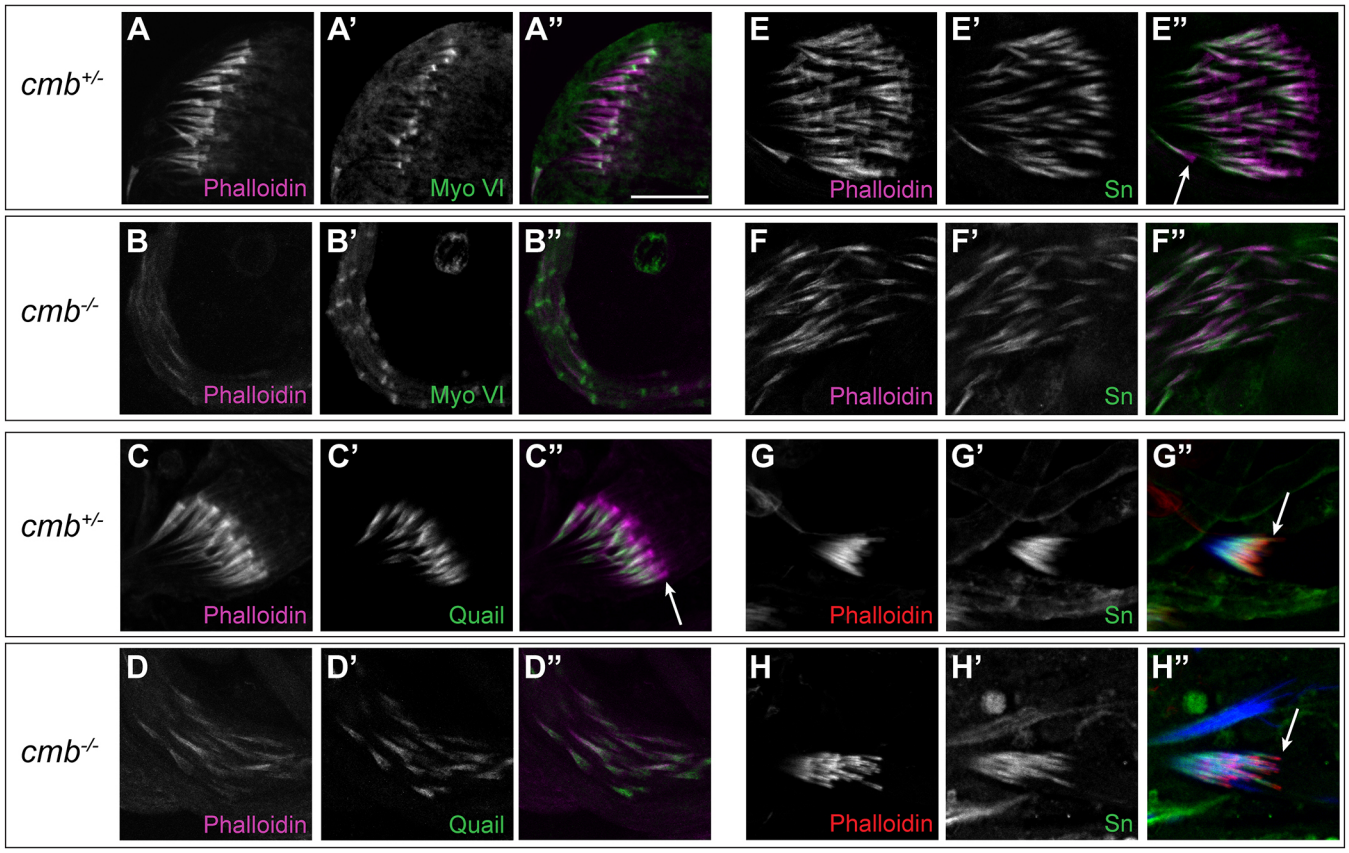

Fig. 6. *cmb* mutant actin cones have normal distribution of actin-binding proteins even when actin structure is abnormal. (A-B″) In heterozygous siblings (A-A″) and cmb^{KO} mutant (B-B″) ICs, Myosin VI (green) marks the front flat edges (mesh) of the actin cones, even in those cones with severely reduced phalloidin staining (purple, B). (C-D″) Quail (green) localizes to the rear actin bundles of control (C-C″) and cmb^{KO} mutant (D-D″) actin cones. (E-F″) Sn (green) also localizes to the rear actin bundles of control (E-E″) and cmb^{KO} (F-F″) mutant actin cones. The *cmb* mutant cones in D and F appear to lack phalloidin staining (purple) in their front flat edges (compare with sibling controls, C″ and E″, arrows). (G-H″) Nascent ICs still associated with spermatid nuclei (DAPI, blue) in the basal testis have front edges that stain prominently with phalloidin (red, arrows) and rear bundles that stain with Sn (green) in both control (G-G″) and cmb^{KO} mutant (H-H″). Scale bar: 20 µm.

of a *dsh* cDNA under control of its endogenous promoter (Fig. S6C,D). We then assessed individualization in testes directly. Mutants of *fz*, *Vang*, and the pk^{1} and $sple^{1}$ alleles of the *pk* gene showed 8-11 normal ICs per testis on average (Fig. 8, quantified in 8I), and fewer than 10% of ICs in each mutant had abnormal morphology (Fig. 8J), consistent with the range of normal ICs seen in various control genotypes (Ben-David et al., 2015). The *dgo* mutant showed fewer normal ICs compared with controls (Fig. 8C,I), but no increase in the number of abnormal ICs (Fig. 8J). Thus, unlike *cmb*, the core PCP genes *fz*, *Vang*, *pk* and *dgo* are not required for IC progression. In the dsh^{1} mutant, testes were short (Fig. 8B), and 21% of ICs that were present were abnormal (Fig. 8I,J; note that the number of normal ICs and WBs, but not the percentage of normal ICs, could be partially rescued; Fig. S6E,F), resembling the normal WBs found at the apical ends of spermatid tails in wild type. This suggests that *dsh* is required for spermatid elongation rather than individualization per se. Likewise, *mwh*, the PPE gene in the wing, was not required for male fertility or spermatid individualization (Fig. 8H-J; Fig. S6A, B). Although *cmb* antagonizes *mwh* during wing hair formation, as reflected by the suppression of the *mwh* MHC phenotype in *mwh cmb* double mutants, *mwh* does not alter the fertility of *cmb* males (Fig. S6A,B). Thus, *cmb* acts independently of the PCP pathway in the testis and likely downstream of distinct signaling pathways in different developmental contexts.

DISCUSSION

The role of Rho kinase in spermatogenesis

Originally, Cmb was identified in a genome-wide screen for Rho kinase (Rok) substrates (Fagan et al., 2014). Rok stimulates the actin cytoskeleton in multiple ways. Activated by RhoA, Rok phosphorylates Myosin II regulatory light chain and Myosin phosphatase, both leading to an increase of actin/myosin contractility (reviewed by Amano et al., 2010; Rath and Olson, 2012; Riento and Ridley, 2003). In addition, Rok's phosphorylation of Lim kinase results in inhibition of cofilin and concomitant stabilization of actin. As mentioned above, we were unable to directly assess a function of RhoA and Rok during spermatogenesis. However, we found that, in contrast to wild type, a version of Cmb in which the five Rok phosphorylation sites identified on Cmb *in vitro* (Fagan et al., 2014) were mutated to alanine fails to rescue the phenotype of *cmb* mutants (Fig. 3E), even though it was expressed in a similar pattern to the wild-type transgene in the developing testes (Fig. S2). It is thus appealing to speculate that Rok may activate Cmb during spermatogenesis. This is distinct from the wing, where an inhibitory relationship was suggested by *Rok* loss of function dominantly enhancing the MHC phenotype caused by Cmb overexpression (Fagan et al., 2014). Therefore, different functions of Cmb in distinct tissues may be controlled differently by Rok. Alternatively, Rok affects wing hair formation in multiple ways (Winter et al., 2001), and thus the genetic interaction detected

Development (2019) 146, dev179275. doi:10.1242/dev.179275

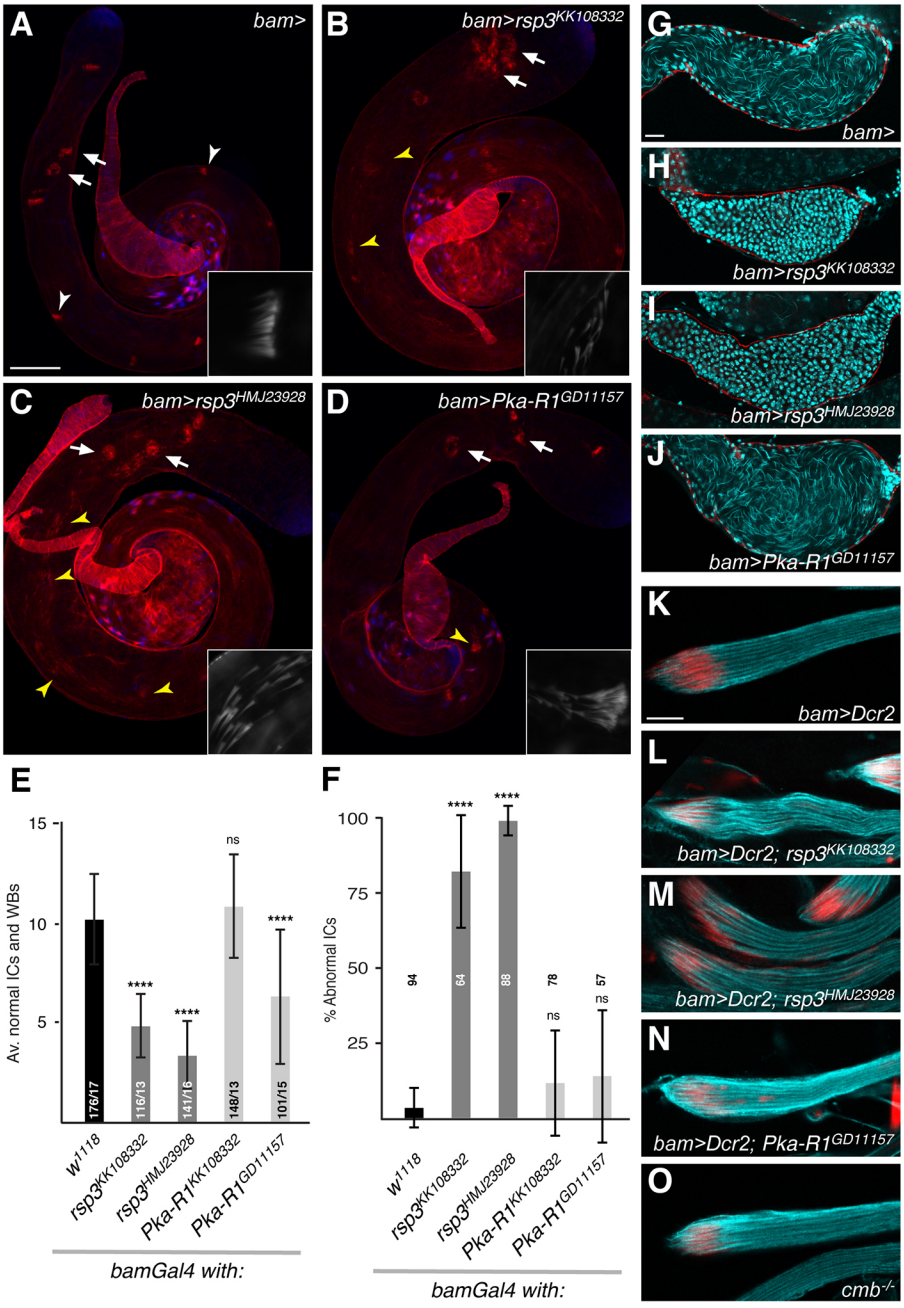

Fig. 7. RNAi knockdown of the Cmb interactors *rsp3* and *Pka-R1* shows similar individualization phenotypes as loss of *cmb*. (A-D) Compared with *bam-GAL4* alone (A), knockdown of *rsp3* (CG32392) with two non-overlapping RNAi constructs causes significant reduction of normal ICs (white arrowheads) and WBs (white arrows) (B,C; quantified in E) and scattering of ICs (yellow arrowheads in B,C; quantified in F). Knockdown of *Pka-R1* with one of the two RNAi constructs (GD11157) reduces the number of normal ICs and WBs, but does not significantly affect the percentage of abnormal ICs under the conditions tested (D, quantified in E and F, respectively). Insets show enlargements of representative aberrant ICs. (E) Quantification of normal ICs and WBs. Numbers on bars indicate number of ICs and WBs counted/number of testes. One-way ANOVA $P<0.0001$; Dunnett's multiple comparison tests ****$P<0.0001$. (F) Quantification of percentage of abnormal ICs. Numbers above bars indicate total structures counted. Non-parametric ANOVA (Kruskal–Wallis); ****$P<0.0001$. ns, not significant. (G-J) Compared with control (G), seminal vesicles of males in which *rsp3* is knocked down with RNAi lines KK108332 (H) or HMJ23928 (I) fail to accumulate mature sperm (DAPI, cyan; phalloidin, red). Mature sperm are found in seminal vesicles of Pka-R1 knockdown males (J). (K-O) Acetylated α-tubulin staining of stable MTs (cyan) is normal in elongated spermatids of *rsp3* (L,M) and *Pka-R1* (N) knockdown, and *cmb* mutant (O) animals (compare with *bam>UAS-Dcr2* control animals in K). DAPI showing nuclei is in red. Scale bars: 100 µm (A-D); 20 µm (G-J); 10 µm (K-O).

in the wing may result from integration of several effects on more than one Rok phosphorylation target.

The PCP pathway in spermatogenesis

Orthologs of the PCP proteins Dsh and Vang are emerging as important regulators of mammalian spermatogenesis. For instance, knockdown of PCP proteins Vangl2 or Dvl1-3 in rat leads to defects in transport and maturation of sperm across the seminiferous epithelium due to disrupted actin and microtubule cytoskeletons in somatic Sertoli cells, which results at least in part from altered expression of cytoskeletal regulatory proteins (Chen and Cheng, 2016; Chen et al., 2016; Chen et al., 2018; Li et al., 2019). To our knowledge, no male fertility phenotype has been reported for PCP genes in *Drosophila*. As Cmb physically and genetically interacts with PCP effectors (Fagan et al., 2014), we tested whether PCP genes show a testis phenotype. We found that dsh^1 and dgo^{380} alleles show a mildly reduced number of normal ICs but only dsh^1 mutants show reduced male fertility. Interestingly, though, the phenotype of dsh^1 mutant males, shorter testes, differs from the reduced actin content and IC scattering found in *cmb* mutants. The *dsh* phenotype is thus likely mechanistically distinct from *cmb* and possibly also from classical PCP signaling, as Fz, the key PCP receptor, is expressed at much lower levels in testes than in imaginal discs and *fz* mutants show no obvious spermatogenesis defects (Fig. S5, Fig. 8). Our data do not distinguish whether Dsh acts in the soma or germline. PCP proteins also regulate ciliogenesis in numerous vertebrate cell types (Adler and Wallingford, 2017; Mirvis et al., 2018). The short testes observed in dsh^1 mutants may suggest a role in biogenesis of the axoneme, a primary cilium, but future work will be required to determine how Dsh affects *Drosophila* spermatogenesis in detail.

Development (2019) 146, dev179275. doi:10.1242/dev.179275

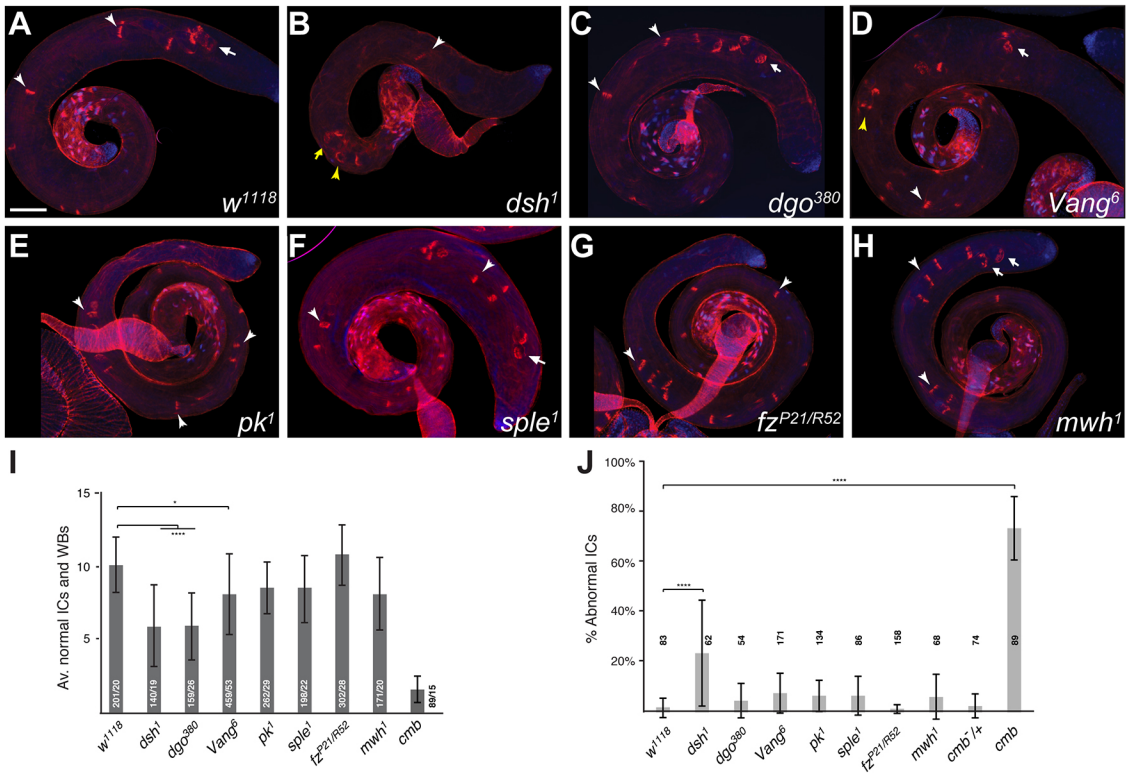

Fig. 8. PCP mutants do not show individualization phenotypes similar to *cmb* mutants. (A-H) w^{1118} and testes of indicated PCP mutants stained with phalloidin (red) to highlight ICs and DAPI (blue, nuclei). White arrowheads and arrows depict normal ICs and WBs, respectively; yellow arrowheads and arrows abnormal ones. Scale bar: 100 µm. (I) Quantification of average number of normal ICs and WBs in the indicated genotypes. dsh^1 and dgo^{380} mutants show fewer normal ICs and WBs per testis than wild type, *Vang* mutants have slightly fewer normal ICs and WBs than wild type. *pk*, *sple*, *fz* and *mwh* mutants are not statistically different from wild type. Data for *cmb* mutants are repeated from Fig. 3 for comparison. Numbers on bars indicate number of total ICs and WBs/number of testes scored. Error bars represent s.d. (J) Percentage of abnormal ICs out of total ICs counted in I. I: one-way ANOVA (P<0.0001) and Tukey's multiple comparison tests; J: non-parametric ANOVA (Kruskal–Wallis) P<0.0001; *P<0.05; ****P<0.0001.

Cmb as a link between IC progression and the axonemes during spermatid individualization

Because Cmb was identified as affecting actin organization in response to PCP signaling in the wing (Fagan et al., 2014), we hypothesized that the male sterility of *cmb* mutants could be due to an actin defect in sperm. Indeed, our results demonstrate that Cmb is essential in the male germline for the actin-dependent process of spermatid individualization. In the *cmb* mutant, ICs organize themselves normally with roughly normal actin levels around the compacted basal spermatid nuclei (Fig. 5A-C). However, as they progress, they present with numerous defects, the most obvious of which is the scattering of actin cones within individual ICs. Close inspection reveals structural defects within the cones as well, including strikingly reduced actin accumulation in both the cone fronts and the rear bundles. However, in *cmb* mutant cones, the rear bundling proteins Quail and Singed (Noguchi et al., 2008), as well as Myosin VI, an important component of the cone fronts (Rogat and Miller, 2002), localize fairly normally (Fig. 6). Therefore, we conclude that *cmb* is important for structural integrity of the entire cone during IC migration rather than for cone polarization.

Several models can be envisaged for Cmb function, the simplest being that Cmb could influence actin recruitment to and/or stability within the ICs by interacting directly with actin. This is, however, unlikely, as we do not detect actin-binding activity in either of two *in vitro* assays, although it is possible that Cmb requires a co-factor to interact with actin. Interestingly, two-hybrid assays and our CoIPs have shown that Cmb can interact with the *Drosophila* homolog of Rsp3, a crucial component of the radial spokes extending from each outer MT doublet towards the central MT pair (Hu et al., 2017). Radial spokes are important for regulation of the flagellar waveform beating movement, and *Chlamydomonas* Rsp3 mutants (*pf14*) were identified by their paralyzed flagella containing a regular 9+2 complement of MTs but lacking radial spokes (Luck et al., 1977; Porter and Sale, 2000; Witman et al., 1978; Yang et al., 2006). In *Drosophila*, similar to *cmb* mutants, germline Rsp3 knockdown results in highly penetrant IC defects, a phenotype that recently has been confirmed in *rsp3* mutants (Wang et al., 2019). We were unable to examine flagellar motility in *cmb* mutants and *rsp3* knockdown animals owing to the complete absence of mature sperm (Fig. 7). Despite a reported interaction with Pka-R1 and individualization defects upon its knockdown, we were unable to confirm the physical interaction by CoIPs (not shown). We cannot discern at present whether this is biologically meaningful or due to technical reasons.

The similarities between the loss of *cmb* and the *rsp3* knockdowns strongly suggest that Cmb helps to coordinate IC movement and stability along the axoneme tracks. To the best of our knowledge, no such link has yet been identified. Although expected, the requirement of the axonemes for IC movement is controversial. No individualization defects are found in Fragile X-related mutants (*Fmr1*) even though their axonemes progressively lose the central MT pair during sperm maturation (Zhang et al., 2004). Likewise, *kl-3* and *kl-5* (Y chromosome dynein heavy chain genes) mutants lack axonemal outer dynein arms but show normal individualization

Development (2019) 146, dev179275. doi:10.1242/dev.179275

(Timakov and Zhang, 2000; Zhang and Stankiewicz, 1998), although in those mutants sperm degenerate later. In contrast, individualization defects are found in sperm with reduced axonemal polyglycylation upon knockdown of the glycylase TTLL3b. Loss of polyglycylation on axonemal MTs is accompanied by severe, but variable, progressive loss of MT structures (Rogowski et al., 2009). Although we cannot exclude radial spoke-independent functions of Rsp3 (Yan et al., 2015), it is thus plausible that ICs need the axonemal MTs as tracks to move along the flagella and may become unstable when they are aberrant. At this time, we do not know whether Cmb plays an active role in the actin cones or rather a permissive role on the axonemes for IC progression. Intriguingly, we detect overexpressed FLAG-tagged Cmb-PA decorating the axonemes in elongation-stage cysts (Fig. S2D). However, despite the ability of the transgene to rescue the individualization defects of *cmb* mutants (Fig. 3), we were not able to evaluate Cmb localization in individualization-stage cysts, likely because of the reduced expression from the *bam-GAL4* driver in later stages.

Overall, we show that the PPE gene *cmb* is required in the germline for proper IC stability and movement along axonemes during sperm individualization. This function is independent of the PCP pathway, but likely requires phosphorylation by Rok. Although the actin-rich IC structure is apparently unique to *Drosophila* sperm, an analogous actin- and microtubule-dependent process of cytoplasmic extrusion likely occurs during spermiation in mammals (Li et al., 2018, 2017; Qian et al., 2014). Furthermore, the sperm axoneme has long been an accessible primary cilium model, and the interplay between cilia and actin (and membrane) dynamics is just beginning to be appreciated (Adler and Wallingford, 2017; Inaba and Mizuno, 2016; Mirvis et al., 2018).

MATERIALS AND METHODS

Fly strains

cmb^{KO}, *UAS-cmb-RA* and *UAS-cmb-RB* have been previously described (Fagan et al., 2014). pTFW (UAS)-cmb-RA6A was made by cloning the mutated fragment of pGEX-4T3-ES (Fagan et al., 2014) into pENTR_3C_cmb_RA and transferring the insert into pTFW via Gateway cloning (Invitrogen). w^{1118}, *tj-GAL4*, UAS-Rho1.N19$^{1.3}$ (BL#7327) and *Rok* (TRiP GL00209) and CG32392/rsp3 (TRiP HMJ23928) RNAi lines were from Bloomington Stock Center. RNAi lines targeting *Rok* (KK107802), *rsp3/CG32392* (KK108322; VDRC#100592), Pka-R1 RNAi (KK101172; VDRC#103720 and GD11157; VDRC#26329) were from the Vienna *Drosophila* Resource Center. dsh^{1}, a PCP-specific allele of *dsh*, dgo^{380}, $Vang^{6}$, pk^{1}, $sple^{1}$, fz^{P21}, fz^{R52} and mwh^{1} (a kind gift of Dr P. Adler, University of Virginia) were described previously (Fagan et al., 2014; Jenny et al., 2005). UASp-Venus:Rok^{K116A} and *bam-GAL4-VP16* were gifts of Drs J. Zallen (Memorial Sloan Kettering Cancer Center, New York, NY, USA) and Y. Yamashita (Life Science Institute, University of Michigan, MI, USA), respectively.

Fertility tests

For sterility tests, single 3- to 5-day-old males were mated with two virgin females of w^{1118} for 3 days on standard fly food supplemented with live yeast grains before parents were discarded. Crosses were scored by whether or not adult offspring eclosed and by counting the number of progeny.

Electron microscopy

Testes were dissected from up to 1-week-old males in PBS and then transferred to fixation buffer overnight (2.5% gluteraldehyde in 0.1 M sodium cacodylate buffer). Samples were then post-fixed with 1% osmium tetroxide followed by 2% uranyl acetate, dehydrated through a graded series of ethanol and embedded in LX112 resin (LADD Research Industries). Ultrathin sections were cut on a Leica Ultracut UC7, stained with uranyl acetate followed by lead citrate and viewed on a JEOL 1200EX transmission electron microscope at 80 kV.

Actin-binding assays

CoIPs were carried out as previously published, transfecting HEK293 cells with 3 µg of each plasmid per 6 cm plate (Fagan et al., 2014). pCDNA3-Act:4-V5 expressing *C. elegans act-4* was a kind gift of Dr H. Bülow, Einstein. GST fusion proteins were expressed as described (Jenny et al., 2003, 2005), except that *Escherichia coli* were lysed in a lysis buffer consisting of 20 mM Tris pH 7.6, 50 mM KCl, 2 mM $MgCl_2$, 1 mM EDTA, 1 mM DTT, and protease inhibitors. Wash buffer additionally contained 0.1% Triton X-100. Proteins were dialyzed against 20 mM Tris pH 7.6, 50 mM KCl, 2 mM $MgCl_2$, 1 mM DTT, 0.1% Triton X-100, 10% glycerol. Actin-pelleting assays were performed using the Actin Binding Protein Kit as indicated by the manufacturer (Cytoskeleton) using 10 µl of the indicated protein (16-30 µg). Note that GST-SX, although soluble after centrifugation at 10,000 ***g*** is not soluble after the 1 h spin at 150,000 g used to preclear the proteins prior to the actin-binding assay.

CoIP assays

Rsp3 was amplified from GH13213 using primers CG32392_for_Sal (GTCGACGCCACCATGCCAGAGACGGAGCAGCAG) and CG32392_rev_Sal (GTCGACTTAGAGATGAGGAGCCGGTGG) using Cloneamp HiFi polymerase (Takara) and cloned into pCR8-GW (Invitrogen). The insert was then transferred into pCS3-Myc6 (Villefranc et al., 2007) using a Clonase LR reaction. Transfections and CoIPs were carried out as published (Fagan et al., 2014) using HEK293 cells (ATCC CRL-1573).

qPCR analyses

For qPCR, testes without accessory glands (but mostly including seminal vesicles) of 20 males were dissected in PBS, washed three times with PBS and then lysed in 0.8 ml Trizol (Invitrogen), according to instructions by the manufacturer. For comparison, RNA of a mix of eye, wing and leg discs from third instar larvae was prepared. Reverse transcription was performed with a Superscript IV first-strand synthesis system (Thermo Fisher Scientific) according to the instructions of the manufacturer. Real-time PCR reactions were performed using the Master cycler Eppendorf realplex^{2} with Power SYBR Green PCR Master Mix (Thermo Fisher Scientific). An equal amount of cDNA was mixed with 5 pmol primers and power green SYBR master mix to make 25 µl of reaction volume. Following 15 min at 95°C for enzyme activation, cycling conditions were: 94°C for 15 s, 30 s at 60°C, 45 s at 72°C for 45 cycles. Melting curve program was 95°C for 15 s, 60°C for 15 s and 95°C for 15 s. Relative expression levels are plotted using the ΔCT method normalizing to the average expression of *RpL11* and *Gapdh2* (Schmittgen and Livak, 2008). Primers used for qPCR are listed in Table S1.

Fluorescence staining and imaging

For whole-mount staining, testes from 0- to 5-day-old males reared at 23°C were dissected in PBS, fixed in 5% formaldehyde in PBX (PBS+0.1% Triton X-100) for 20 min, and washed in PBX. For immunofluorescence, a 1 h block was performed in 5% normal donkey serum (Jackson ImmunoResearch) +1% Triton X-100 before overnight incubation with primary antibodies. Testes were stained with TRITC-phalloidin (Sigma-Aldrich, P1951) together with secondary antibodies and mounted in DAPI-Fluoromount G (Southern Biotech). IC quantification was performed as described by Ben-David et al. (2015).

For immunostaining of actin-cone proteins, ring canals, and acetylated α-tubulin, testes were squashed on slides and frozen in liquid N_2 before fixation and staining, as described by Sitaram et al. (2014).

Primary antibodies were mouse anti-α-Spectrin [Developmental Studies Hybridoma Bank (DSHB), 3A9, 1:25], rabbit anti-cleaved caspase-3 (Cell Signaling Technology, 9664T, 1:100), mouse anti-Myosin VI (gift of K. Miller, Washington University, St. Louis, MO, USA; 3C7, 1:20), mouse anti-Quail (DSHB, 6B9, 1:50), mouse anti-Sn (DSHB, sn7C, undiluted), mouse anti-phospho-Tyrosine (Abcam, ab10321, 1:200), mouse anti-acetylated α-tubulin (Sigma-Aldrich, 6-11B-1, 1:100), and mouse anti-FLAG (Sigma-Aldrich, M2, 1:500). Donkey secondary antibodies (Jackson ImmunoResearch 711-545-152 or Molecular Probes A21202) were used at 1:200.

Testes were imaged using an Olympus IX-81 motorized inverted microscope with XM-10 monochrome camera (lenses: 10×/0.3 NA, 20×/0.75 NA, 40×oil/1.3 NA, 60× oil/1.35 NA), a Zeiss LSM510 confocal microscope (lenses: 10×/0.3 NA, 20×/0.8 NA, 40×/0.75 NA) or a Zeiss LSM800 confocal microscope (lenses: 10×/0.3 NA, 20×/0.8 NA, 40× oil/1.3 NA). Intensity of ICs was quantified from epifluorescence images of phalloidin-stained testes using Fiji/ImageJ as follows: regions of interest of five ICs still associated with nuclei from five testes per genotype were selected and average fluorescence was tabulated. Quantifying integrated density gave qualitatively similar results.

For phase-contrast imaging of post-meiotic spermatids, testes were squashed onto slides in PBS and imaged live with phase contrast within 30 min using an Olympus IX-71 inverted microscope with DS-U2 Nikon camera and NIS Elements software (20× lens/0.40 NA).

Acknowledgements
We are grateful to our colleagues for sharing reagents, including P. Adler, J. Zallen, Y. Yamashita, and K. Miller, to Leslie Gunther of the Einstein AIF for help with EM (National Institutes of Health grant P30CA013330), and to Dr Mimi Kim (Einstein Department of Epidemiology & Population Health) for advice on statistics. We thank the Bloomington *Drosophila* Stock Center (National Institutes of Health P40OD018537), Vienna *Drosophila* Resource Center, and Developmental Studies Hybridoma Bank (created by the NICHD of the NIH and maintained at The University of Iowa, Department of Biology, Iowa City, IA) for fly stocks and reagents. We are grateful to Steinhauer lab students Tzvi Fishkin and Aryeh Korman, who helped generate preliminary data for the project. We thank Drs J. Secombe, J. Treisman, H. Bülow and J. Rollins for their comments on this manuscript.

Competing interests
The authors declare no competing or financial interests.

Author contributions
Conceptualization: J.S., A.J.; Methodology: J.S., B.S., J.K.F., J.B., S.S., P.Y., D.E., A.J.; Validation: J.S., A.J.; Formal analysis: J.S., A.J.; Investigation: J.S., B.S., J.K.F., J.B., S.S., P.Y., D.E., A.J.; Resources: J.S., A.J.; Data curation: J.S., A.J.; Writing - original draft: J.S., A.J.; Writing - review & editing: J.S., A.J.; Supervision: J.S., A.J.; Funding acquisition: J.S., A.J.

Funding
Work in the Steinhauer lab is supported by a Eunice Kennedy Shriver National Institute of Child Health and Human Development grant (R15HD080511) and in the Jenny lab by National Institute of General Medical Sciences grants (GM115646, GM088202). Deposited in PMC for release after 12 months.

Supplementary information
Supplementary information available online at
http://dev.biologists.org/lookup/doi/10.1242/dev.179275.supplemental

References
Adler, P. N. and Wallingford, J. B. (2017). From planar cell polarity to ciliogenesis and back: the curious tale of the PPE and CPLANE proteins. *Trends Cell Biol.* **27**, 379-390. doi:10.1016/j.tcb.2016.12.001

Adler, P. N., Zhu, C. and Stone, D. (2004). Inturned localizes to the proximal side of wing cells under the instruction of upstream planar polarity proteins. *Curr. Biol.* **14**, 2046-2051. doi:10.1016/j.cub.2004.11.007

Amano, M., Nakayama, M. and Kaibuchi, K. (2010). Rho-kinase/ROCK: A key regulator of the cytoskeleton and cell polarity. *Cytoskeleton* **67**, 545-554. doi:10.1002/cm.20472

Arama, E., Agapite, J. and Steller, H. (2003). Caspase activity and a specific cytochrome C are required for sperm differentiation in Drosophila. *Dev. Cell* **4**, 687-697. doi:10.1016/S1534-5807(03)00120-5

Bazinet, C. and Rollins, J. E. (2003). Rickettsia-like mitochondrial motility in Drosophila spermiogenesis. *Evol. Dev.* **5**, 379-385. doi:10.1046/j.1525-142X.2003.03045.x

Ben-David, G., Miller, E. and Steinhauer, J. (2015). Drosophila spermatid individualization is sensitive to temperature and fatty acid metabolism. *Spermatogenesis* **5**, e1006089. doi:10.1080/21565562.2015.1006089

Butler, M. T. and Wallingford, J. B. (2017). Planar cell polarity in development and disease. *Nat. Rev. Mol. Cell Biol.* **18**, 375-388. doi:10.1038/nrm.2017.11

Chen, H. and Cheng, C. Y. (2016). Planar cell polarity (PCP) proteins and spermatogenesis. *Semin. Cell Dev. Biol.* **59**, 99-109. doi:10.1016/j.semcdb.2016.04.010

Chen, H., Mruk, D. D., Lee, W. M. and Cheng, C. Y. (2016). Planar cell polarity (PCP) protein Vangl2 regulates ectoplasmic specialization dynamics via its effects on actin microfilaments in the testes of male rats. *Endocrinology* **157**, 2140-2159. doi:10.1210/en.2015-1987

Chen, H., Xiao, X., Lui, W.-Y., Lee, W. M. and Cheng, C. Y. (2018). Vangl2 regulates spermatid planar cell polarity through microtubule (MT)-based cytoskeleton in the rat testis. *Cell Death Dis.* **9**, 340. doi:10.1038/s41419-018-0339-x

Fabian, L. and Brill, J. A. (2012). Drosophila spermiogenesis: Big things come from little packages. *Spermatogenesis* **2**, 197-212. doi:10.4161/spmg.21798

Fabrizio, J. J., Hime, G., Lemmon, S. K. and Bazinet, C. (1998). Genetic dissection of sperm individualization in Drosophila melanogaster. *Development* **125**, 1833-1843.

Fagan, J. K., Dollar, G., Lu, Q., Barnett, A., Pechuan Jorge, J., Schlosser, A., Pfleger, C., Adler, P. and Jenny, A. (2014). Combover/CG10732, a novel PCP effector for Drosophila wing hair formation. *PLoS ONE* **9**, e107311. doi:10.1371/journal.pone.0107311

Fuller, M. (1993). Spermatogenesis. In *The Development of Drosophila Melanogaster* (ed. M. Bate and A. Martinez Arias), pp. 71-148. Cold Spring Harbor Laboratory Press.

Gaillard, A. R., Diener, D. R., Rosenbaum, J. L. and Sale, W. S. (2001). Flagellar radial spoke protein 3 is an A-kinase anchoring protein (AKAP). *J. Cell Biol.* **153**, 443-448. doi:10.1083/jcb.153.2.443

Gaillard, A. R., Fox, L. A., Rhea, J. M., Craige, B. and Sale, W. S. (2006). Disruption of the A-kinase anchoring domain in flagellar radial spoke protein 3 results in unregulated axonemal cAMP-dependent protein kinase activity and abnormal flagellar motility. *Mol. Biol. Cell* **17**, 2626-2635. doi:10.1091/mbc.e06-02-0095

Ghosh-Roy, A., Kulkarni, M., Kumar, V., Shirolikar, S. and Ray, K. (2004). Cytoplasmic dynein-dynactin complex is required for spermatid growth but not axoneme assembly in Drosophila. *Mol. Biol. Cell* **15**, 2470-2483. doi:10.1091/mbc.e03-11-0848

Greenbaum, M. P., Iwamori, T., Buchold, G. M. and Matzuk, M. M. (2011). Germ cell intercellular bridges. *Cold Spring Harb. Perspect Biol.* **3**, a005850. doi:10.1101/cshperspect.a005850

Hermo, L., Pelletier, R. M., Cyr, D. G. and Smith, C. E. (2010a). Surfing the wave, cycle, life history, and genes/proteins expressed by testicular germ cells. Part 2: changes in spermatid organelles associated with development of spermatozoa. *Microsc. Res. Tech.* **73**, 279-319. doi:10.1002/jemt.20787

Hermo, L., Pelletier, R. M., Cyr, D. G. and Smith, C. E. (2010b). Surfing the wave, cycle, life history, and genes/proteins expressed by testicular germ cells. Part 3: developmental changes in spermatid flagellum and cytoplasmic droplet and interaction of sperm with the zona pellucida and egg plasma membrane. *Microsc. Res. Tech.* **73**, 320-363. doi:10.1002/jemt.20784

Hu, Y., Perrimon, N., Vidal, M. and Celniker, S. (2017). FlyBi (BDGP/CCSB/DRSC) preliminary fly interactome data. http://flybi.hms.harvard.edu/results.php.

Huang, B., Piperno, G., Ramanis, Z. and Luck, D. J. (1981). Radial spokes of Chlamydomonas flagella: genetic analysis of assembly and function. *J. Cell Biol.* **88**, 80-88. doi:10.1083/jcb.88.1.80

Huh, J. R., Vernooy, S. Y., Yu, H., Yan, N., Shi, Y., Guo, M. and Hay, B. A. (2004). Multiple apoptotic caspase cascades are required in nonapoptotic roles for Drosophila spermatid individualization. *PLoS Biol.* **2**, E15. doi:10.1371/journal.pbio.0020015

Inaba, K. and Mizuno, K. (2016). Sperm dysfunction and ciliopathy. *Reprod Med. Biol.* **15**, 77-94. doi:10.1007/s12522-015-0225-5

Jenny, A., Darken, R. S., Wilson, P. A. and Mlodzik, M. (2003). Prickle and Strabismus form a functional complex to generate a correct axis during planar cell polarity signaling. *EMBO J.* **22**, 4409-4420. doi:10.1093/emboj/cdg424

Jenny, A., Reynolds-Kenneally, J., Das, G., Burnett, M. and Mlodzik, M. (2005). Diego and Prickle regulate Frizzled planar cell polarity signalling by competing for Dishevelled binding. *Nat. Cell Biol.* **7**, 691-697. doi:10.1038/ncb1271

Jivan, A., Earnest, S., Juang, Y.-C. and Cobb, M. H. (2009). Radial spoke protein 3 is a mammalian protein kinase A-anchoring protein that binds ERK1/2. *J. Biol. Chem.* **284**, 29437-29445. doi:10.1074/jbc.M109.048181

Li, L., Tang, E. I., Chen, H., Lian, Q., Ge, R., Silvestrini, B. and Cheng, C. Y. (2017). Sperm release at spermiation is regulated by changes in the organization of actin- and microtubule-based cytoskeletons at the apical ectoplasmic specialization-a study using the adjudin model. *Endocrinology* **158**, 4300-4316. doi:10.1210/en.2017-00660

Li, L., Mao, B., Wu, S., Lian, Q., Ge, R.-S., Silvestrini, B. and Cheng, C. Y. (2018). Regulation of spermatid polarity by the actin- and microtubule (MT)-based cytoskeletons. *Semin. Cell Dev. Biol.* **81**, 88-96. doi:10.1016/j.semcdb.2018.01.013

Li, L., Mao, B., Yan, M., Wu, S., Ge, R., Lian, Q. and Cheng, C. Y. (2019). Planar cell polarity protein Dishevelled 3 (Dvl3) regulates ectoplasmic specialization (ES) dynamics in the testis through changes in cytoskeletal organization. *Cell Death Dis.* **10**, 194. doi:10.1038/s41419-019-1394-7

Lu, Q., Schafer, D. A. and Adler, P. N. (2015). The Drosophila planar polarity gene multiple wing hairs directly regulates the actin cytoskeleton. *Development* **142**, 2478-2486. doi:10.1242/dev.122119

Luck, D., Piperno, G., Ramanis, Z. and Huang, B. (1977). Flagellar mutants of Chlamydomonas: studies of radial spoke-defective strains by dikaryon and

revertant analysis. *Proc. Natl. Acad. Sci. USA* **74**, 3456-3460. doi:10.1073/pnas.74.8.3456

Maung, S. M. T. W. and Jenny, A. (2011). Planar cell polarity in Drosophila. *Organogenesis* **7**, 165-179. doi:10.4161/org.7.3.18143

Mermall, V., Bonafé, N., Jones, L., Sellers, J. R., Cooley, L. and Mooseker, M. S. (2005). Drosophila myosin V is required for larval development and spermatid individualization. *Dev. Biol.* **286**, 238-255. doi:10.1016/j.ydbio.2005.07.028

Mészáros, B., Erdős, G. and Dosztányi, Z. (2018). IUPred2A: context-dependent prediction of protein disorder as a function of redox state and protein binding. *Nucleic Acids Res.* **46**, W329-W337. doi:10.1093/nar/gky384

Mirvis, M., Stearns, T. and James Nelson, W. (2018). Cilium structure, assembly, and disassembly regulated by the cytoskeleton. *Biochem. J.* **475**, 2329-2353. doi:10.1042/BCJ20170453

Noguchi, T. and Miller, K. G. (2003). A role for actin dynamics in individualization during spermatogenesis in Drosophila melanogaster. *Development* **130**, 1805-1816. doi:10.1242/dev.00406

Noguchi, T., Lenartowska, M. and Miller, K. G. (2006). Myosin VI stabilizes an actin network during Drosophila spermatid individualization. *Mol. Biol. Cell* **17**, 2559-2571. doi:10.1091/mbc.e06-01-0031

Noguchi, T., Lenartowska, M., Rogat, A. D., Frank, D. J. and Miller, K. G. (2008). Proper cellular reorganization during Drosophila spermatid individualization depends on actin structures composed of two domains, bundles and meshwork, that are differentially regulated and have different functions. *Mol. Biol. Cell* **19**, 2363-2372. doi:10.1091/mbc.e07-08-0840

Porter, M. E. and Sale, W. S. (2000). The 9+2 axoneme anchors multiple inner arm dyneins and a network of kinases and phosphatases that control motility. *J. Cell Biol.* **151**, F37-F42. doi:10.1083/jcb.151.5.F37

Qian, X., Mruk, D. D., Cheng, Y.-H., Tang, E. I., Han, D., Lee, W. M., Wong, E. W. and Cheng, C. Y. (2014). Actin binding proteins, spermatid transport and spermiation. *Semin. Cell Dev. Biol.* **30**, 75-85. doi:10.1016/j.semcdb.2014.04.018

Rath, N. and Olson, M. F. (2012). Rho-associated kinases in tumorigenesis: re-considering ROCK inhibition for cancer therapy. *EMBO Rep.* **13**, 900-908. doi:10.1038/embor.2012.127

Riento, K. and Ridley, A. J. (2003). Rocks: multifunctional kinases in cell behaviour. *Nat. Rev. Mol. Cell Biol.* **4**, 446-456. doi:10.1038/nrm1128

Rogat, A. D. and Miller, K. G. (2002). A role for myosin VI in actin dynamics at sites of membrane remodeling during Drosophila spermatogenesis. *J. Cell Sci.* **115**, 4855-4865. doi:10.1242/jcs.00149

Rogowski, K., Juge, F., van Dijk, J., Wloga, D., Strub, J.-M., Levilliers, N., Thomas, D., Bré, M.-H., Van Dorsselaer, A., Gaertig, J. et al. (2009). Evolutionary divergence of enzymatic mechanisms for posttranslational polyglycylation. *Cell* **137**, 1076-1087. doi:10.1016/j.cell.2009.05.020

Schmittgen, T. D. and Livak, K. J. (2008). Analyzing real-time PCR data by the comparative C(T) method. *Nat. Protoc.* **3**, 1101-1108. doi:10.1038/nprot.2008.73

Siddall, N. A. and Hime, G. R. (2017). A Drosophila toolkit for defining gene function in spermatogenesis. *Reproduction* **153**, R121-R132. doi:10.1530/REP-16-0347

Sitaram, P., Hainline, S. and Lee, L. (2014). Cytological analysis of spermatogenesis: live and fixed preparations of Drosophila testes. *J. Vis. Exp.* **83**, e51058. doi:10.3791/51058

Steinhauer, J. (2015). Separating from the pack: molecular mechanisms of spermatid individualization. *Spermatogenesis* **5**, e1041345. doi:10.1080/21565562.2015.1041345

Strutt, D. and Warrington, S. J. (2008). Planar polarity genes in the Drosophila wing regulate the localisation of the FH3-domain protein Multiple Wing Hairs to control the site of hair production. *Development* **135**, 3103-3111. doi:10.1242/dev.025205

Thurmond, J., Goodman, J. L., Strelets, V. B., Attrill, H., Gramates, L. S., Marygold, S. J., Matthews, B. B., Millburn, G., Antonazzo, G., Trovisco, V. et al. (2019). FlyBase 2.0: the next generation. *Nucleic Acids Res.* **47**, D759-D765. doi:10.1093/nar/gky1003

Timakov, B. and Zhang, P. (2000). Genetic analysis of a Y-chromosome region that induces triplosterile phenotypes and is essential for spermatid individualization in Drosophila melanogaster. *Genetics* **155**, 179-189.

Tokuyasu, K. T. (1975). Dynamics of spermiogenesis in Drosophila melanogaster. VI. Significance of “onion” nebenkern formation. *J. Ultrastruct. Res.* **53**, 93-112. doi:10.1016/S0022-5320(75)80089-X

Tokuyasu, K. T., Peacock, W. J. and Hardy, R. W. (1972a). Dynamics of spermiogenesis in Drosophila melanogaster. I. Individualization process. *Z. Zellforsch. Mikrosk. Anat.* **124**, 479-506. doi:10.1007/BF00335253

Tokuyasu, K. T., Peacock, W. J. and Hardy, R. W. (1972b). Dynamics of spermiogenesis in Drosophila melanogaster. II. Coiling process. *Z. Zellforsch. Mikrosk. Anat.* **127**, 492-525. doi:10.1007/BF00306868

Villefranc, J. A., Amigo, J. and Lawson, N. D. (2007). Gateway compatible vectors for analysis of gene function in the zebrafish. *Dev. Dyn.* **236**, 3077-3087. doi:10.1002/dvdy.21354

Wang, Y., Xu, R., Cheng, Y., Cao, H., Wang, Z., Zhu, T., Jiang, J., Zhang, H., Wang, C., Qi, L. et al. (2019). RSBP15 interacts with and stabilizes dRSPH3 during sperm axoneme assembly in Drosophila. *J. Genet. Genomics* **46**, 281-290. doi:10.1016/j.jgg.2019.05.001

White-Cooper, H. (2012). Tissue, cell type and stage-specific ectopic gene expression and RNAi induction in the Drosophila testis. *Spermatogenesis* **2**, 11-22. doi:10.4161/spmg.19088

Winter, C. G., Wang, B., Ballew, A., Royou, A., Karess, R., Axelrod, J. D. and Luo, L. (2001). Drosophila Rho-associated kinase (Drok) links Frizzled-mediated planar cell polarity signaling to the actin cytoskeleton. *Cell* **105**, 81-91. doi:10.1016/S0092-8674(01)00298-7

Wirschell, M., Zhao, F., Yang, C., Yang, P., Diener, D., Gaillard, A., Rosenbaum, J. L. and Sale, W. S. (2008). Building a radial spoke: flagellar radial spoke protein 3 (RSP3) is a dimer. *Cell Motil. Cytoskeleton* **65**, 238-248. doi:10.1002/cm.20257

Witman, G. B., Plummer, J. and Sander, G. (1978). Chlamydomonas flagellar mutants lacking radial spokes and central tubules. Structure, composition, and function of specific axonemal components. *J. Cell Biol.* **76**, 729-747. doi:10.1083/jcb.76.3.729

Yan, R., Hu, X., Zhang, W., Song, L., Wang, J., Yin, Y., Chen, S. and Zhao, S. (2015). The mouse radial spoke protein 3 is a nucleocytoplasmic shuttling protein that promotes neurogenesis. *Histochem. Cell Biol.* **144**, 309-319. doi:10.1007/s00418-015-1338-y

Yang, P., Diener, D. R., Yang, C., Kohno, T., Pazour, G. J., Dienes, J. M., Agrin, N. S., King, S. M., Sale, W. S., Kamiya, R. et al. (2006). Radial spoke proteins of Chlamydomonas flagella. *J. Cell Sci.* **119**, 1165-1174. doi:10.1242/jcs.02811

Zhang, P. and Stankiewicz, R. L. (1998). Y-Linked male sterile mutations induced by P element in Drosophila melanogaster. *Genetics* **150**, 735-744.

Zhang, Y. Q., Matthies, H. J. G., Mancuso, J., Andrews, H. K., Woodruff, E., III, Friedman, D. and Broadie, K. (2004). The Drosophila fragile X-related gene regulates axoneme differentiation during spermatogenesis. *Dev. Biol.* **270**, 290-307. doi:10.1016/j.ydbio.2004.02.010

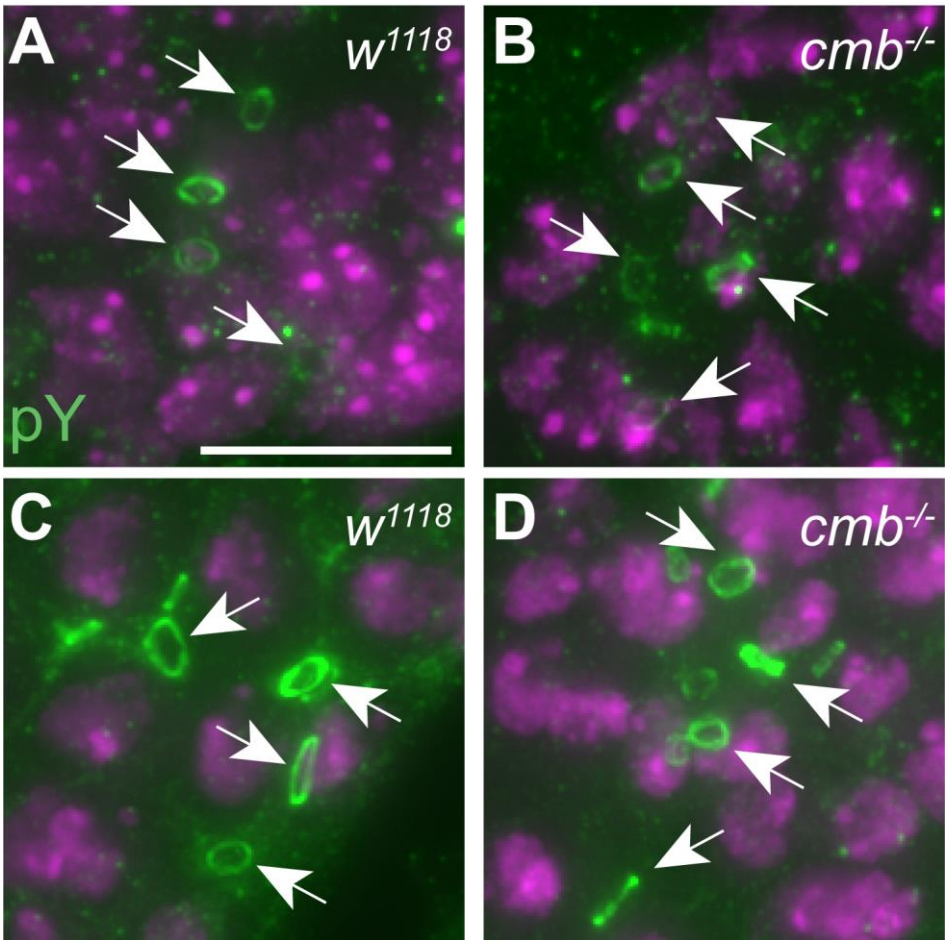

Figure S1. Ring canals are normal in *cmb* mutants. Ring canals (arrows) stained by α-phospho-tyrosine (green) appear normal in spermatogonia of *cmb* mutants (B, D, compare to spermatogonia of w^{1118} controls in A, C). Nuclei are marked with DAPI (purple). Maximal intensity projections of squashed testes (stacks with 15-45 0.27 μm optical sections). Scale bar: 10μm.

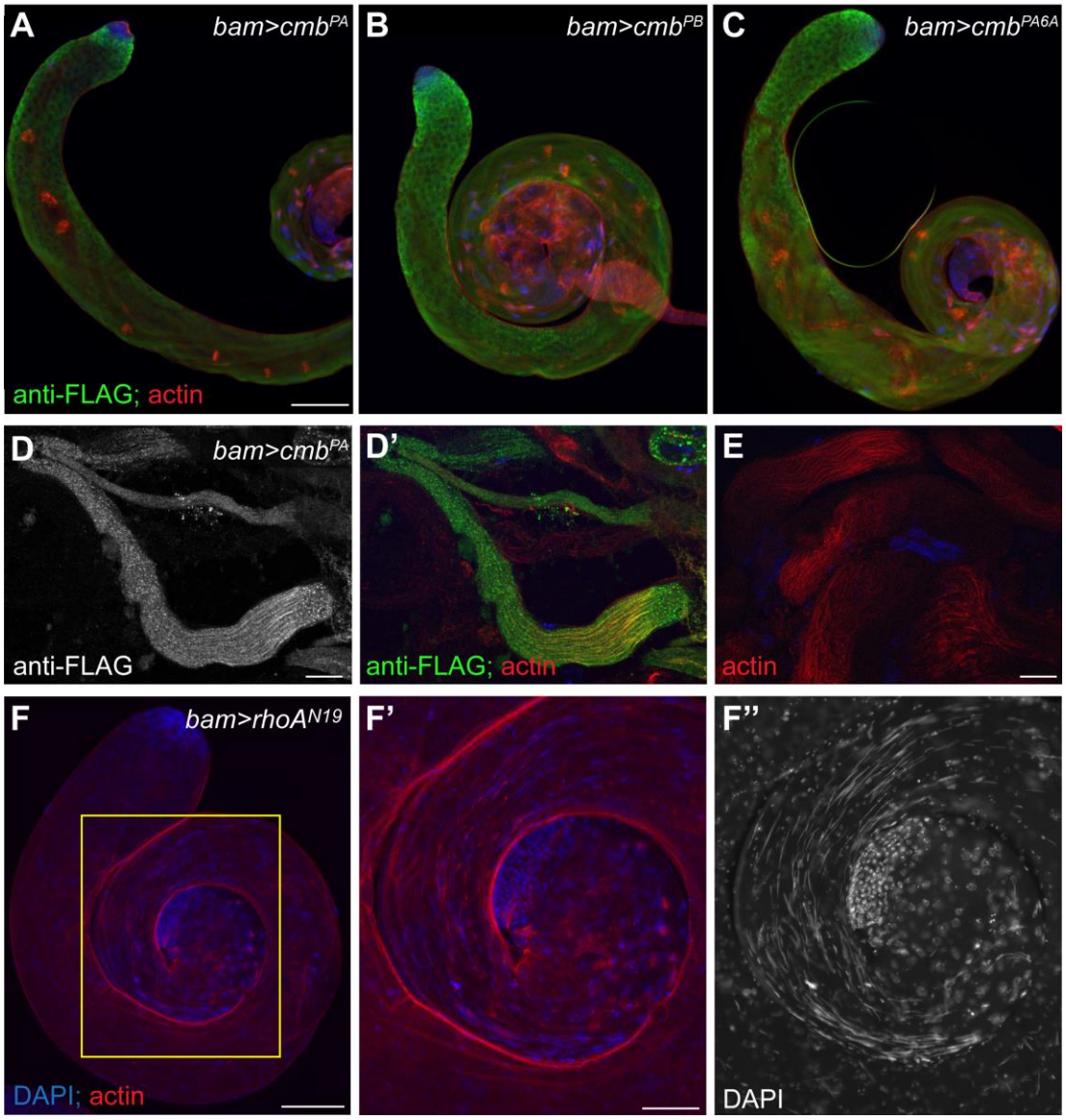

Figure S2. Rescue transgene expression. Anti-FLAG staining (green) shows expression of Cmb-PA (A), Cmb-PB (B), and Cmb-PA6A (C) in the germline with *bam-GAL4.* ICs are marked with phalloidin (red), nuclei with DAPI (blue). Scale bar 100 µm. (D) Anti-FLAG staining (grayscale in D, green in D') of squashed testes expressing Cmb-PA with *bam-GAL4* reveals Cmb-PA decorating the axonemes in elongation stage cysts. Control staining without the anti-FLAG primary antibody shown in E (control staining performed alongside and photographed with identical settings as experimental). Scale bar: 20 µm. (F) Dominant negative RhoA^{N19} causes scattering of nuclei as well as actin cones (area outlined in yellow is enlarged in F'; actin cones are marked with phalloidin (red), nuclei with DAPI (blue); F'' shows DAPI alone). Scale bars: 100 µm (F) and 50 µm (F').

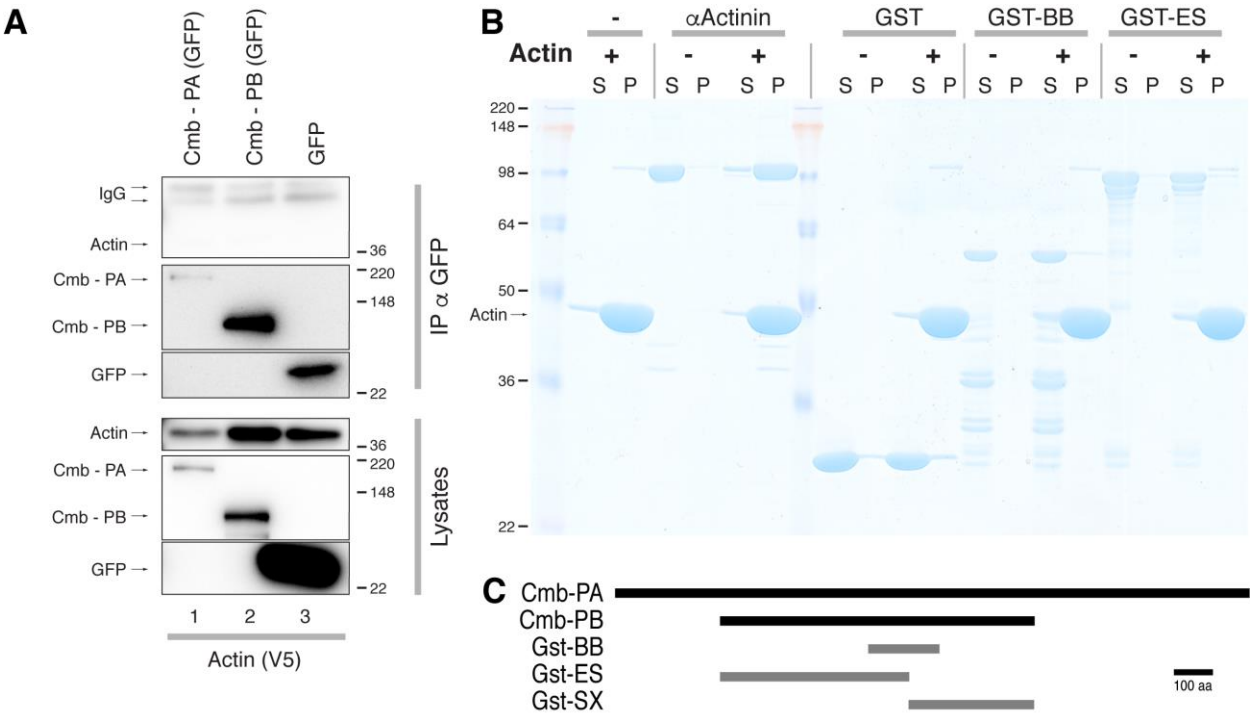

Figure S3. Cmb does not co-precipitate or co-sediment with actin. (A) Co-immunoprecipitation assays show that neither GFP tagged Cmb-PA, GFP-Cmb-PB nor GFP precipitates *C. elegans* V5-tagged Act4. Immunoprecipitations are shown in the upper panels, lysates in the lower panels as marked on the right. Migration positions of each protein and relevant molecular mass markers are indicated on the left and right, respectively. Note that GFP-Cmb, while expressed judged by GFP positive cells in culture, only transfers inefficiently onto Western membranes. (B) Actin co-sedimentation assays with restriction enzyme based sub-fragments of Cmb (see also schematic in C). Supernatants (S) and pellets (P) of the co-sedimentation assays of the proteins indicated on top in the presence (+) or absence (-) of F-actin. In contrast to αActinin that is found in the pellet fraction in the presence of actin, neither GST nor GST-BB or GST-ES fragments of Cmb are co-pelleted with actin. (C) Schematic of Cmb protein variants used.

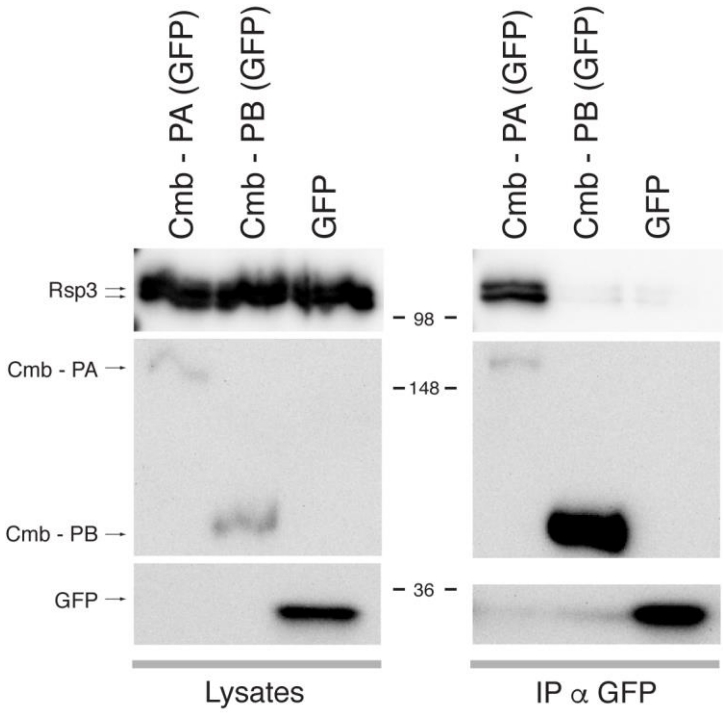

Figure S4. Cmb-PA interacts with Rsp3. Western blot of CoIPs from HEK293 transfected with Myc6-tagged Rsp3 together with plasmids indicated on top. Proteins detected on the Western are indicated on the left. Left panels: cell lysates; right panels: proteins immunoprecipitated with GFP antibodies.

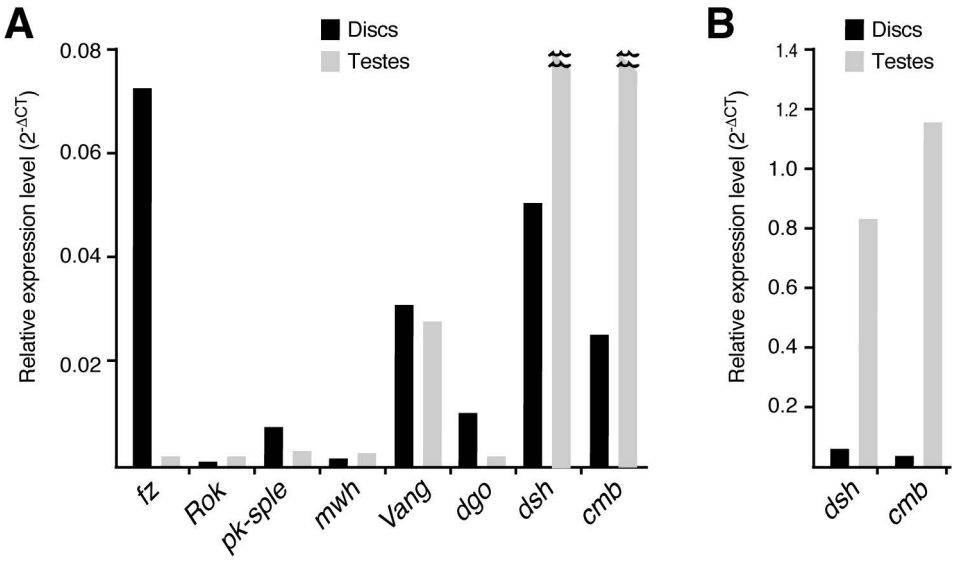

Figure S5. qPCR results depicting relative expression of PCP genes in testes compared to eye, wing, and leg discs normalized to the average of *Gapdh2* and *RpL11*(A). *fz* and *dgo* and to a lesser extent, *pk*, are expressed at lower levels in testes compared to imaginal discs. In contrast to *Rok, Vang/stbm, and mwh* that are expressed at comparable levels, *dsh* and *cmb* are expressed at much higher levels in testes (shown with different scale in B).

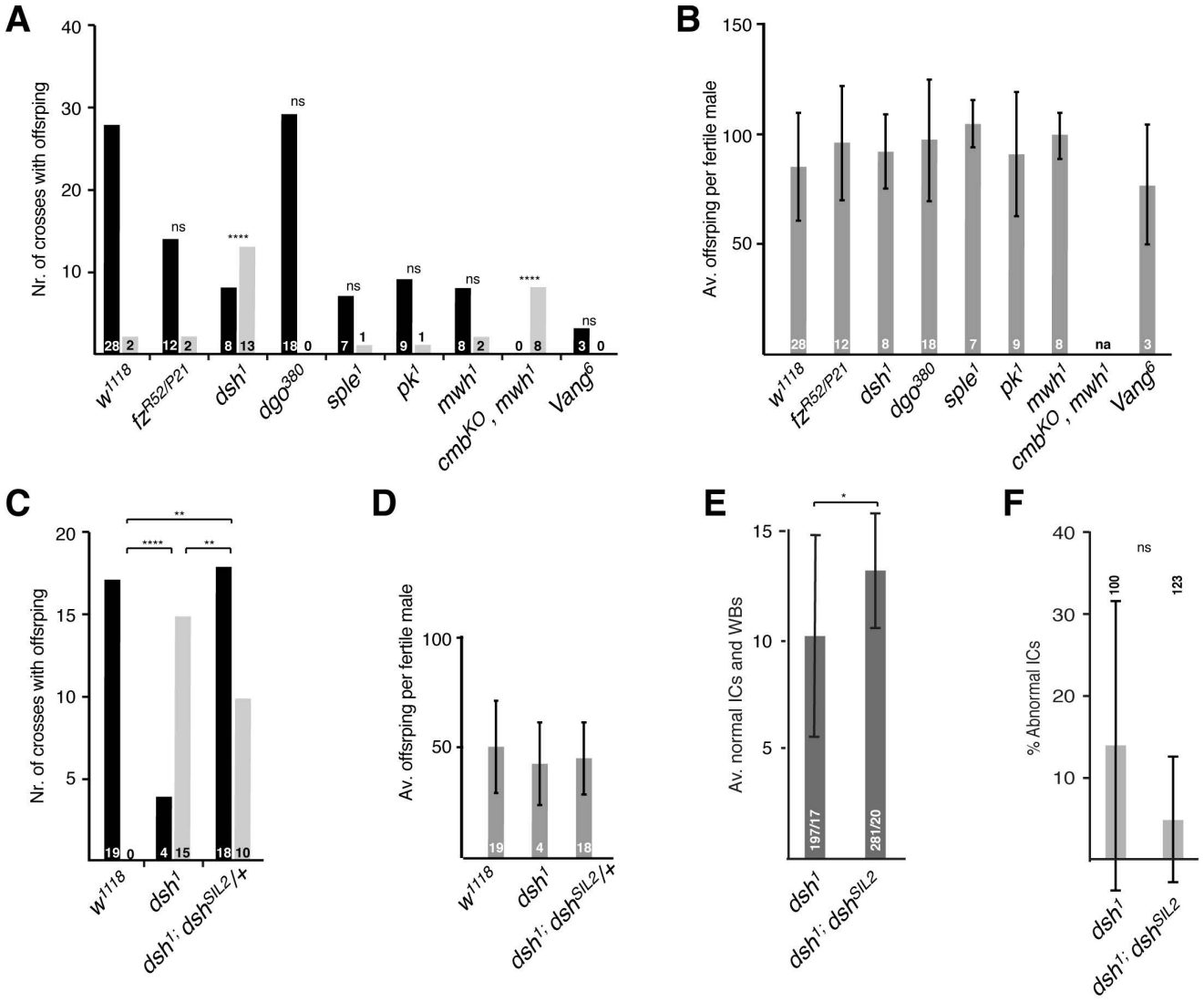

Figure S6. Male fertility of PCP mutants. (A) Number of single male crosses that were fertile (black bars) or that produced no offspring (grey bars). (B) Average numbers of offspring from fertile crosses of (A). (C-F) Rescue of the *dsh*^{1} allele with a dsh promoter driven dsh cDNA. (C) Number of single male crosses that were fertile (black bars) or that produced no offspring (grey bars) of indicated genotypes. The fertility defects *dsh*^{1} mutant is partially rescued. (D) Average numbers of offspring from fertile crosses of (C). (E, F) The average number of normal ICs and waste bags (E), but not the percentage of abnormal ICs (F), is partially rescued by expression of *dsh* under its endogenous promoter. A,C: ** p<0.01; **** p<0.0001, Two-sided Fisher's exact test. E: p<0.05; unpaired T-test. F: ns: not significant; Mann-Whitney test (non-parametric). Error bars indicate standard deviation; na: not applicable.

Table S1. qPCR primers

dsh Forward primer	Dsh_for_RT	TACTGCCCTGCTTCAATGGG
dsh Reverse primer	Dsh_Rev_RT	ACCCATGCCCAATTCACACT
fz Forward primer	Fz_For_RT	TAAACACCAGACGGGCGTAG
fz Reverse primer	Fz_Rev_RT	CATGCAGATCCTTTCCGCCA
mwh Forward primer	mwh_For_rt	GCGCGGGTGTTAAATTTCTC
*mw*h Reverse primer	mwh_Rev_rt	ATGGTACGAGCCAAGGTGCT
pk Forward primer	Prickle_For_RT	GGCCTGCGATGAGATTATCC
pk Reverse primer	Prickle_Rev_RT	AGTCGCAGTACTCGGCAAAC
Rok Forward primer	Rok_For_RT	GACCTGCCCAAACAAAAGAACA
Rok Reverse primer	Rok_Rev_RT	GCAGCTGGTTGAACTTGTCG
Vang Forward primer	Vang_For_RT	GAGATGCTTTGCTCCGAGGT
Vang Reverse primer	Vang_Rev_RT	ATATGACAGGAGACGGCAGC
dgo Forward primer	Diego_For_RT	GTCCGGAATAATTATGGAGATACTC
dgo Reverse primer	Diego_Rev_RT	TGTCGCCGTTCAGATTTGTT
cmb Forward primer	cmb_For_RT	CCGGATCGAATGCCTCTACC
cmb Reverse primer	cmb_Rev_RT	CGATCCTGGAGCGCATGTAG
Gapdh2 Forward primer	GAPDH-2_For_RT	CTACCTGTTCAAGTTCGATTCGAC
Gapdh2 Reverse primer	GAPDH-2_Rev_RT	AGTGGACTCCACGATGTATTCG
RpL11 Forward primer	Rpl11_For_RT	CTGGGCATCAAGTACGATCC
RpL11 Reverse primer	Rpl11__Rev_RT	AACCACTTCATGGCATCCTC